

1 **Identifying fire plumes in the Arctic with tropospheric FTIR**  
2 **measurements and transport models**

3 C. Viatte<sup>1,\*</sup>, K. Strong<sup>1</sup>, J. Hannigan<sup>2</sup>, E. Nussbaumer<sup>2</sup>, L. K. Emmons<sup>2</sup>, S. Conway<sup>1</sup>, C. Paton-Walsh<sup>3</sup>, J.  
4 Hartley<sup>1</sup>, J. Benmergui<sup>4,\*\*</sup>, and J. Lin<sup>4,5</sup>

5 <sup>1</sup>Department of Physics, University of Toronto, Toronto, ON, Canada

6 <sup>2</sup>National Center for Atmospheric Research, Boulder, CO, USA

7 <sup>3</sup>Department of Chemistry, University of Wollongong, Wollongong, New South Wales, Australia

8 <sup>4</sup>Department of Earth and Environmental Sciences, University of Waterloo, Waterloo, ON,

9 Canada

10 <sup>5</sup>Department of Atmospheric Sciences, University of Utah, Salt Lake City, UT, USA

11 \*now at: Division of Geological and Planetary Sciences, California Institute of Technology, Pasadena,  
12 CA, USA

13 \*\*now at: School of Engineering and Applied Sciences, Harvard University, Cambridge, MA, USA

14

15 **Abstract**

16 We investigate Arctic tropospheric composition using ground-based Fourier Transform Infrared  
17 (FTIR) solar absorption spectra, recorded at the Polar Environment Atmospheric Research  
18 Laboratory (PEARL, Eureka, Nunavut, Canada, 80°05'N, 86°42'W) and at Thule (Greenland,  
19 76°53'N, -68°74'W) from 2008 to 2012. The target species: carbon monoxide (CO), hydrogen  
20 cyanide (HCN), ethane (C<sub>2</sub>H<sub>6</sub>), acetylene (C<sub>2</sub>H<sub>2</sub>), formic acid (HCOOH), and formaldehyde  
21 (H<sub>2</sub>CO) are emitted by biomass burning and can be transported from mid-latitudes to the Arctic.

22 By detecting simultaneous enhancements of three biomass burning tracers (HCN, CO, and C<sub>2</sub>H<sub>6</sub>),  
23 ten and eight fire events are identified at Eureka and Thule, respectively, within the five-year FTIR  
24 timeseries. Analyses of Hybrid Single Particle Lagrangian Integrated Trajectory Model  
25 (HYSPLIT) back-trajectories coupled with Moderate Resolution Imaging Spectroradiometer  
26 (MODIS) fire hot spot data, Stochastic Time-Inverted Lagrangian Transport model (STILT)  
27 footprints, and Ozone Monitoring Instrument (OMI) UV aerosol index maps are used to attribute  
28 burning source regions and travel time durations of the plumes. By taking into account the effect  
29 of aging of the smoke plumes, measured FTIR enhancement ratios were corrected to obtain  
30 emission ratios and equivalent emission factors. The means of emission factors for extratropical  
31 forest estimated with the two FTIR datasets are:  $0.40 \pm 0.21 \text{ g kg}^{-1}$  for HCN,  $1.24 \pm 0.71 \text{ g kg}^{-1}$  for  
32 C<sub>2</sub>H<sub>6</sub>,  $0.34 \pm 0.21 \text{ g kg}^{-1}$  for C<sub>2</sub>H<sub>2</sub>, and  $2.92 \pm 1.30 \text{ g kg}^{-1}$  for HCOOH. The emission factor for  
33 CH<sub>3</sub>OH estimated at Eureka is  $3.44 \pm 1.68 \text{ g kg}^{-1}$ .

34 To improve our knowledge concerning the dynamical and chemical processes associated with  
35 Arctic pollution from fires, the two sets of FTIR measurements were compared to the Model for  
36 Ozone and Related chemical Tracers, version 4 (MOZART-4). Seasonal cycles and day-to-day  
37 variabilities were compared to assess the ability of the model to reproduce emissions from fires  
38 and their transport. Good agreement in winter confirms that transport is well implemented in the  
39 model. For C<sub>2</sub>H<sub>6</sub>, however, the lower wintertime concentration estimated by the model as  
40 compared to the FTIR observations highlight an underestimation of its emission. Results show that  
41 modelled and measured total columns are correlated (linear correlation coefficient  $r > 0.6$  for all  
42 gases except for H<sub>2</sub>CO at Eureka and HCOOH at Thule), but suggest a general underestimation of  
43 the concentrations in the model for all seven tropospheric species in the high Arctic.

## 44 **1) Introduction**

45 Fires release trace gases into the atmosphere, affecting air quality (Colarco et al., 2004), climate,  
46 and the carbon cycle (IPCC, 2007). Those radiatively and photochemically active trace gases  
47 include carbon monoxide (CO), hydrogen cyanide (HCN), and Non-Methane HydroCarbons  
48 (NMHCs), including ethane (C<sub>2</sub>H<sub>6</sub>), acetylene (C<sub>2</sub>H<sub>2</sub>), methanol (CH<sub>3</sub>OH), formic acid (HCOOH),  
49 and formaldehyde (H<sub>2</sub>CO) (Paton-Walsh et al., 2010; Akagi et al., 2011; Vigouroux et al., 2012).  
50 Given their long atmospheric lifetimes, CO, HCN, and C<sub>2</sub>H<sub>6</sub> are considered to be tracers of long-  
51 range pollution transport associated with biomass burning plumes. In the Arctic, these gases and  
52 the other shorter-lived species (C<sub>2</sub>H<sub>2</sub>, CH<sub>3</sub>OH, HCOOH, and H<sub>2</sub>CO) affect tropospheric chemistry  
53 (Generoso et al., 2007, Stohl et al., 2007, Tilmes et al., 2011), oxidizing power (Mao et al., 2010;  
54 Olson et al., 2012), and radiative transfer (Wang et al., 2011) of this sensitive polar region, which  
55 has been warming rapidly over the past century (Lesins et al., 2010). Since fire frequency and  
56 intensity are sensitive to climate change and variability, as well as land use practices (Kasischke  
57 et al., 2006; Soja et al., 2007; IPCC, 2007; Amiro et al., 2009; Flannigan et al. 2009; Oris et al.,  
58 2013; Kelly et al., 2013), they constitute a large source of variability in Arctic tropospheric  
59 composition.

60 Biomass burning plumes transported over the Arctic have been observed by ground-based Fourier  
61 Transform InfraRed (FTIR) spectrometers (Yurganov et al., 2004, 2005 ; Viatte et al., 2013),  
62 measurements on aircraft (Paris et al., 2009; Warneke et al., 2009; Simpson et al., 2011; Hecobian  
63 et al., 2011; Parrington et al., 2013; O'Shea et al., 2013; Le Breton et al., 2013; Lewis et al., 2013),  
64 and satellites (Rinsland et al., 2007; Coheur et al., 2009; Tereszchuk et al., 2011; Tereszchuk et  
65 al., 2013). Model simulations and meteorological analyses also suggest pollution transport  
66 pathways to the Arctic (Eckhardt et al., 2003; Klonecki et al., 2003; Koch and Hansen, 2005; Stohl  
67 et al., 2006; Shindell et al., 2008; Thomas et al., 2013; Bian et al., 2013). However, our knowledge  
68 concerning transport, degradation mechanisms of NMHCs (Stavrakou et al., 2009), sources of  
69 Arctic pollution (Fisher et al., 2010), and emissions from fires (Akagi et al., 2011) remains  
70 incomplete, reflecting the heterogeneous and stochastic nature of these processes. Long-term and  
71 continuous measurements of Arctic tropospheric composition are therefore important for  
72 quantifying emissions from fire plumes transported from lower latitudes and improving the  
73 prediction of trace gas concentrations and variability in chemical transport model simulations. This  
74 would help in assessing the atmospheric impact of biomass burning pollution on the Arctic climate  
75 system.

76 To simulate fire emissions in chemical transport models, emission factors of various trace gases  
77 must be estimated with accuracy. Emission factors are highly variable however, because they  
78 depend on the types of vegetation burned, the combustion phase (smoldering and flaming), and  
79 atmospheric conditions at the time of the fire events (Paton-Walsh et al., 2005, 2008, 2010; Akagi  
80 et al., 2011; Hornbrook et al., 2011; Vigouroux et al., 2012). Within the past decade, measurements  
81 of emission factors of biomass burning species have led to a wide range of values, which may be  
82 due to the natural variability of the emissions and/or the discrepancies between sampling methods  
83 (laboratory, airborne, satellite, and ground-based measurements) that overestimate or  
84 underestimate the combustion phases (smoldering and flaming). The need for more measurements  
85 of HCN and NMHC emission factors has been stressed given the value of HCN as a biomass  
86 burning tracer (Li et al., 2003), and significant NMHC emissions from fires (Andreae and Merlet,  
87 2001; Akagi et al., 2011; Paulot et al., 2011; Wiedinmyer et al., 2011).

88 We investigate pollution from biomass burning events that occurred in extratropical forests and  
89 were transported to the high Arctic with two sets of FTIR measurements, located at Eureka  
90 (Nunavut, Canada, 80°05'N, -86°42'W) and Thule (Greenland, 76°53'N, -68°74'W). Seven  
91 tropospheric species (CO, HCN, C<sub>2</sub>H<sub>6</sub>, C<sub>2</sub>H<sub>2</sub>, CH<sub>3</sub>OH, HCOOH, and H<sub>2</sub>CO) released by biomass  
92 burning were monitored from 2008 to 2012. Complete descriptions of the methodologies and  
93 characterizations of the retrievals are found in Viatte et al. (2014). These species were selected  
94 because of their differing anthropogenic, biogenic, fossil fuel burning and biomass burning source  
95 fractions, as well as their widely differing lifetimes, sinks, and secondary production rates. From  
96 this diversity we gain insight into chemistry and transport abilities of the Model for Ozone and  
97 Related chemical Tracers, version 4 (MOZART-4, Emmons et al., 2010) and improve emission  
98 ratios. A significant number of observations inside fire plumes are identified in the datasets, and  
99 used to derive emission ratios (and hence infer emission factors) of the target species. These  
100 measured emission ratios add new values to the sparse dataset reported in the literature. The two  
101 sets of measurements are compared with MOZART-4 to assess the ability of this model to  
102 reproduce Arctic tropospheric chemical composition and its variability due to the long-range  
103 pollution transport from fires.

104

## 105 2) Observations and model data in the high Arctic

### 106 2.1) FTIR measurements at Eureka and Thule

107 We present measurements over five years of seven tropospheric species in the high Arctic: CO,  
108 HCN, C<sub>2</sub>H<sub>6</sub>, C<sub>2</sub>H<sub>2</sub>, CH<sub>3</sub>OH, HCOOH, and H<sub>2</sub>CO, from 2008 to 2012. These timeseries are  
109 obtained from ground-based FTIR measurements performed at Eureka (80°05'N, 86°42'W, 0.61  
110 km above sea level, Eureka, Nunavut, Canada, Fogal et al., 2013) and Thule (76°53'N, -68°74'W,  
111 0.23 km above sea level, Greenland, Thule, Hannigan et al., 2009). The locations of the  
112 measurement sites are shown in Figure 1. The high-resolution solar absorption spectrometers (a  
113 Bruker IFS 125HR at Eureka and a Bruker IFS 120M at Thule, both operated at a spectral  
114 resolution of 0.0035 cm<sup>-1</sup>) are part of the international Network for the Detection of Atmospheric  
115 Composition Change (NDACC, <http://www.ndsc.ncep.noaa.gov/>, formerly NDSC, Kurylo, 1991;  
116 Kurylo and Zander 2001). These spectrometers measure spectra using two detectors (Indium  
117 Antimonide - InSb - or Mercury Cadmium Telluride - MCT), a potassium bromide (KBr)  
118 beamsplitter, and a sequence of seven and eight narrow-band interference filters covering the 600-  
119 4300 cm<sup>-1</sup> and 750-5000 cm<sup>-1</sup> spectral range, at Eureka and Thule, respectively. A reference low-  
120 pressure hydrogen bromide (HBr) cell spectrum is recorded regularly with an internal global  
121 source to characterize the Instrumental Line Shape (ILS) and monitor alignment of both  
122 instruments (Coffey et al. 1998). By using the LINEFIT software analysis (Hase et al., 1999),  
123 modulation efficiency and phase error are retrieved and can be included in the retrieval analysis  
124 (i.e. forward model).

125  
126 In order to retrieve concentrations of these species from the recorded spectra, the Optimal  
127 Estimation Method (OEM, Rodgers, 2000) has been applied using the new SFIT4 retrieval code  
128 (<https://wiki.ucar.edu/display/sfit4/Infrared+Working+Group+Retrieval+Code%2C+SFIT>). With  
129 the exception of the ILS and Signal to Noise Ratio (SNR), which are specific to each instrument,  
130 we use the same methodology to analyze the Eureka and Thule measurements, i.e., homogenized  
131 micro-windows, the same spectroscopic parameters from the HITRAN 2008 database (Rothman  
132 et al., 2009), and the same *a priori* covariance matrices. For CO, HCN, and C<sub>2</sub>H<sub>6</sub>, retrieval  
133 parameters are based on the NDACC-IRWG standard parameter definitions (NDACC Infrared  
134 Working Group, <http://www.acd.ucar.edu/irwg/>). Details of the retrievals of the seven  
135 tropospheric species at Eureka are described in Viatte et al. (2014). *A priori* profiles of the target  
136 species are derived from the mean of 40-year runs from the Whole Atmosphere Community

137 Climate Model, version 6 (WACCM, <http://www2.cesm.ucar.edu/working-groups>, Garcia et al.,  
138 2007; Eyring et al., 2007), for the two stations. Daily pressure and temperature profiles are from  
139 the National Center for Environment Prediction (NCEP, <http://www.ncep.noaa.gov/>). Monthly *a*  
140 *priori* water vapour profiles are taken from the WACCM output for each location. Our profiles are  
141 retrieved on 48-level altitude grids (from 0.61 to 120 km for Eureka, and from 0.23 to 120 km for  
142 Thule) and total and partial columns are then derived by vertically integrating these profiles.

143 Full error analysis has been performed for both datasets, as described in Rodgers (2000) and  
144 Rodgers and Connors (2003), and includes measurement noise error, smoothing error (expressing  
145 the limited vertical resolution of the retrieval), and forward model parameter error. Details about  
146 the seven tropospheric species error budget can be seen in Viatte et al. (2014) in section 2.6.  
147 Timeseries are obtained from February to October since the FTIR measurements require the sun  
148 as the light source. The seasonal cycles of CO, HCN, C<sub>2</sub>H<sub>6</sub>, C<sub>2</sub>H<sub>2</sub>, CH<sub>3</sub>OH, HCOOH, and H<sub>2</sub>CO  
149 are representative of their differing transport, emissions, lifetimes, and oxidation rates, and have  
150 been discussed in detail in Viatte et al. (2014) with reference to the Eureka dataset.

151 The CO, HCN, and C<sub>2</sub>H<sub>6</sub> total columns measured at Eureka and Thule from 2008 to 2012 are  
152 shown on the left and right panels, respectively, of Figure 2. These species are considered to be  
153 biomass burning tracers, given their long lifetimes in the atmosphere of fifty-two days (Daniel and  
154 Solomon, 1998), five months (Li et al., 2003), and eighty days (Xiao et al., 2008) for CO, HCN,  
155 and C<sub>2</sub>H<sub>6</sub>, respectively. They exhibit strong seasonal cycles, reflecting the importance of chemistry  
156 and transport processes in their Arctic budget. In addition to these cycles, simultaneous  
157 enhancements of the CO, HCN, and C<sub>2</sub>H<sub>6</sub> total columns can be seen in the day-to-day variabilities,  
158 in both Eureka and Thule observations, such as in April and July 2008 (red circles, Figure 2), and  
159 in August 2010 (green squares, Figure 2). Enhancements of CO, HCN, and C<sub>2</sub>H<sub>6</sub> total columns  
160 observed at Thule in June-July 2012 (olive triangles, Figure 2) are not seen in the Eureka dataset  
161 because there were no FTIR measurements at Eureka during this period. Some of these  
162 enhancements have already been attributed to biomass burning plumes transported to the Arctic.  
163 This has been done with aircraft measurements for the April 2008 (Warneke et al., 2009) and July  
164 2008 events (Simpson et al., 2011) during the Arctic Research of the Composition of the  
165 Troposphere from Aircrafts and Satellites (ARCTAS) campaigns (Jacob et al., 2010; Hornbrook  
166 et al., 2011), and with ground-based FTIR measurements for the extreme August 2010 event  
167 (Viatte et al., 2013), as well as with the combination of numerous measurement platforms for the  
168 July 2011 event, during the Quantifying the impact of BOREal forest fires on Tropospheric

169 oxidants over the Atlantic using Aircraft and Satellites (BORTAS) experiment (Palmer et al.,  
170 2013).

171 Figure 3 shows timeseries of C<sub>2</sub>H<sub>2</sub>, CH<sub>3</sub>OH, HCOOH, and H<sub>2</sub>CO total columns measured at  
172 Eureka (left panels) and Thule (right panels) from 2008 to 2012. These species have different  
173 lifetimes in the atmosphere, ranging from two weeks for C<sub>2</sub>H<sub>2</sub> (Xiao et al., 2007) to less than two  
174 days for H<sub>2</sub>CO (Coheur et al., 2007). Because of their possible chemical destruction during long-  
175 range transport to the Arctic, enhancements due to fire events are less significant than for the three  
176 main biomass burning tracers (Figure 2) but are still present in the timeseries, as shown in August  
177 2010 for Eureka (green squares, Figure 3) and in August 2008 for Thule (red circles, Figure 3).  
178 These species have also been measured by Atmospheric Chemistry Experiment - Fourier  
179 Transform Spectrometer (ACE-FTS, Tereszchuk et al., 2013) and Infrared Atmospheric Sounding  
180 Interferometer (IASI, Coheur et al., 2009), as well as aircraft measurements (Parrington et al.,  
181 2013; O'Shea et al., 2013) in boreal forest biomass burning plumes several days after their source  
182 emissions. Indeed, a recent study suggests that the physical age of one boreal plume in July 2011  
183 is 1 to 5 days older than the photochemical age because of the presence of the pyrogenic aerosols  
184 which slow down the plume photochemistry for several days after the emission (Finch et al., 2014).

185 For various reasons, the number of days of observation out of the approximate eight month sunlit  
186 portion of the year at these remote Arctic sites will vary year to year from as few as 15 to many  
187 110. Often days will have multiple observations. For the five-year period (2008-2012), the average  
188 number of measurements per gas shown in Figure 3 is 2149 for Eureka and 868 for Thule.  
189 Although the difference in the number of FTIR measurements throughout the years between the  
190 Eureka and Thule datasets, the timeseries of the seven tropospheric species recorded at both  
191 stations exhibit similar seasonal cycles, in term of absolute values and temporal variabilities. We  
192 can exploit the accuracy of these FTIR retrievals, and the robustness of the multi-year observations  
193 in the quantification of Arctic tropospheric composition and its variability. Super-imposed on these  
194 seasonal cycles, the timeseries reveal short-term enhancements due to fire events that highlight the  
195 importance of the biomass burning long-range transport in the Arctic budget of NMHCs, which  
196 can affect air quality and climate in this region.

## 197 **2.2) MOZART-4 description**

198 MOZART-4 (Model for OZone And Related chemical Tracers), version 4, is a Chemical Transport  
199 Model (CTM) developed jointly by the (US) National Center for Atmospheric Research (NCAR),

200 the Geophysical Fluid Dynamics Laboratory (GFDL), and the Max Planck Institute for  
201 Meteorology (MPI-Met) to simulate atmospheric chemical and transport processes. To assess the  
202 ability of MOZART-4 to reproduce the different seasonal cycles of the seven tropospheric species,  
203 as well as the day-to-day variabilities due to fire signatures, we used daily mean outputs for all of  
204 2008 and a temporal resolution of six hours within four time periods between 2008 to 2012  
205 (Emmons et al., 2010) to compare with the FTIR datasets. Those periods are (1) March to August  
206 2008 to assess the model's seasonal cycles, (2) August to October 2010 to evaluate biomass  
207 burning emissions of the model for the most extreme fire event, as well as (3) May to July 2011,  
208 and (4) June to July 2012 to focus the analyses on other fire events during summer periods.

209 For that specific model run, a comprehensive tropospheric chemistry, including 100 species, 160  
210 kinetic, and 40 photolysis reactions, has been used. The simulations are driven by offline  
211 meteorological data from the Goddard Earth Observing System Model, Version 5 (GEOS-5) and  
212 the Modern Era Retrospective analysis for Research and Applications (MERRA) at  $0.5^{\circ} \times 0.6^{\circ}$  and  
213  $1.9^{\circ} \times 2.5^{\circ}$  resolution with 56 vertical levels. Emissions are taken from the anthropogenic inventory  
214 created for the ARCTAS campaign by David Streets (Argonne National Lab,  
215 <http://bio.cgrer.uiowa.edu/arctas/emission.html>), which is based on several inventories, including  
216 the INTEX-B Asia inventory, the U.S. Environmental Protection Agency (EPA) National  
217 Emission Inventory (NEI), the European Monitoring and Evaluation Programme (EMEP)  
218 inventory, as well as the Emissions Database for Global Atmospheric Research (EDGAR). For  
219 biomass burning emissions, we use the Fire INventory from NCAR (FINN, Wiedinmyer et al.,  
220 2011). FINN is based on MODIS thermal anomalies and is available daily  
221 (<https://www2.acd.ucar.edu/modeling/finn-fire-inventory-ncar>), thus MOZART-4 simulations do  
222 use daily fire emissions. Finally, biogenic emissions are calculated online for isoprene and  
223 terpenes, and offline for methanol, from the Model of Emissions of Gases and Aerosols from  
224 Nature (MEGAN) inventory (Guenther et al., 2012). At the time the simulations were performed,  
225 the significance of biogenic emissions of formic acid was not appreciated, so were not included.  
226 In total, the model has a HCOOH emission of 3.7 Tg/yr, for which 1.1 Tg/yr are for anthropogenic  
227 sources and 3.3 Tg/yr for biomass burning. The estimate of biogenic HCOOH emissions in  
228 MEGAN-v2.1 is 3.7 Tg/yr (Guenther et al., 2012), so inclusion of them would double the current  
229 MOZART-4 emissions.

### 230 **3) Methods and results**

### 3.1) Detection of biomass burning events with FTIR observations in the Arctic

231  
232 We identify fire events in the FTIR timeseries by selecting all days that have simultaneous  
233 enhancements of the three main biomass burning tracers (CO, HCN, and C<sub>2</sub>H<sub>6</sub>). All measurements  
234 which lie beyond three standard deviations of the monthly mean total columns are considered as  
235 biomass burning indicators. This methodology was used in Viatte et al. (2013) and relies on the  
236 assumption that a smoke plume detected in the high Arctic has come from a relatively large fire  
237 and would have large emissions for several consecutive days.

238 With this methodology, ten biomass burning events have been identified as reaching Eureka (Table  
239 1) and eight for Thule (Table 2), from 2008 to 2012. At least five fire events have reached both  
240 sites almost simultaneously in March 2008, July-August 2008, July-August 2010, June-July 2011,  
241 and July 2012.

242 The number of events detected in the high Arctic appears correlated with the boreal forest  
243 temperature (Barrett et al., 2013). In summer 2009, only one event in June 2009 was detected over  
244 Eureka (Table 1). Low temperatures over the boreal forest  
245 ([http://earthobservatory.nasa.gov/GlobalMaps/view.php?d1=MOD14A1\\_M\\_FIRE](http://earthobservatory.nasa.gov/GlobalMaps/view.php?d1=MOD14A1_M_FIRE)) are consistent  
246 with a smaller number of fire events detected at our sites. A recent study of FINN also confirms  
247 the smaller number of boreal fires in 2009 (Wiedinmyer et al., 2011, their Table 7).

248 In order to match the biomass burning candidate events identified in the timeseries with actual  
249 plumes, it is necessary to find the source fires and show that the plumes generated there are capable  
250 of travelling to the Arctic stations where they were observed. This is done by using various  
251 independent datasets:

252 (1) The Air Resources Laboratory (ARL, <http://ready.arl.noaa.gov/hysplit-bin/>) Hybrid Single  
253 Particle Lagrangian Integrated Trajectory Model (HYSPLIT), which generates mean-wind back-  
254 trajectories for air parcels at designated elevations using Global Data Assimilation System  
255 (GDAS) meteorological fields (<https://ready.arl.noaa.gov/gdas1.php>).

256 (2) The source region information in the form of “footprints” from a time-reversed Lagrangian  
257 particle dispersion model, the Stochastic Time-Inverted Lagrangian Transport model (STILT, Lin  
258 et al., 2003; Gerbig et al., 2003) also driven by GDAS meteorological fields. **Trajectories were  
259 initialized at 0, 6, 12, and 18 UTC on 23 above-ground-height levels (ranging from 0.2 to 14.5  
260 km). Each trajectory used 500 particles. Footprints from the different levels were combined as a**

261 weighted mean to create a single footprint that is representative of a column measurement. Weights  
262 were derived as the product of the pressure at the receptor multiplied by the instrument kernel  
263 density (which was linearly interpolated to the receptor height). The trajectories were run 30 days  
264 back in time.

265 (3) The Moderate Resolution Imaging Spectroradiometer (MODIS, [http://lance-](http://lance-modis.eosdis.nasa.gov/cgi-bin/imagery/firemaps.cgi)  
266 [modis.eosdis.nasa.gov/cgi-bin/imagery/firemaps.cgi](http://lance-modis.eosdis.nasa.gov/cgi-bin/imagery/firemaps.cgi)), which captures global fire maps.

267 (4) Satellite images from Ozone Monitoring Instrument (OMI,  
268 [http://gdata1.sci.gsfc.nasa.gov/daac-bin/G3/gui.cgi?instance\\_id=omi](http://gdata1.sci.gsfc.nasa.gov/daac-bin/G3/gui.cgi?instance_id=omi)), which measures UV  
269 aerosol index.

270 In addition, we use AERONET aerosol optical depth (AOD) data measured at Eureka (O'Neill et  
271 al., 2008; Saha et al., 2010; <http://aeronet.gsfc.nasa.gov/>), when available, to detect simultaneous  
272 increase of fine mode AOD and trace gas total columns, which is an additional fire event indicator.  
273 If these data all agree on a common origin for a plume, and the back-trajectories intersect that  
274 region during the same time, then the source of a biomass burning event has been successfully  
275 detected. Consistent results from these multiple datasets provides confidence in the attribution of  
276 trace gas enhancements to specific fire events.

277 Figure 4 shows an example of the source attribution and the travel duration of a plume that reached  
278 Eureka on the 10<sup>th</sup> of July, 2008. We first note a simultaneous enhancement of the three main  
279 biomass burning tracers concentrations detected on the 10<sup>th</sup> of July 2008 at Eureka (see Figure 5).  
280 *As a priori* information, STILT footprints are generated to show the source region influencing the  
281 atmospheric measurement at Eureka, which for that day is located in Eastern Russia (light blue  
282 region inside the red box, Figure 4a). Then the FIRMS map (Fire Information for Resource  
283 Management System, which provides MODIS hot spot data) is used to verify that a significant fire  
284 event occurs in that specific region, within a 10-day period (red dots in Figure 4b). To assess the  
285 travel duration of that plume from the fire region to Eureka, an ensemble of HYSPLIT back-  
286 trajectories is generated, for several travel times, end times of the calculated trajectories, and air-  
287 parcel altitudes, *e. g.* for each biomass burning event detected at a specific time, we ran ten  
288 HYSPLIT backtrajectories for different altitudes ranging from 3 to 12 km, and modified the end  
289 time of these backtrajectories within two hours of the observed enhancements. In Figure 4c,  
290 airmasses ending at Eureka at 5, 7, and 9 km (red, blue, and green lines, respectively) on July 10<sup>th</sup>,  
291 come from the fire region (red box). And finally, the OMI aerosol index map is used to confirm

292 the presence of a significant fire event in that region, as shown in Figure 4d (colored area within  
293 the red box). Similar example of fire source region and travel time attribution can be seen in Viatte  
294 et al. (2013, Figure 2) for the August 2010 event.

295 Using this methodology, four fire plumes were attributed to forest fires in Asia travelling for 7 to  
296 9 days, and six from North America travelling between 5 and 8 days, for Eureka (Table 1). For  
297 Thule, three biomass burning plumes come from Russia after 7 to 9 days of travel and five are  
298 from North America, travelling between 5 and 6 days (Table 2).

299 In addition, because fire emission composition depends upon, among others parameters, the type  
300 of biomass burned (Andreae and Merlet, 2001; Akagi et al., 2011), we assigned the vegetation type  
301 burned (boreal, temperate coniferous and grassland; Olson et al., 2001) for the different fire events  
302 based on the fire source region. This ensured the appropriate selection of the Emission Factor (EF)  
303 of CO needed to calculate the emission factors of the other species from the FTIR measurements  
304 of emission ratios (Section 3.2.2).

305

## 306 **3.2) Evaluation of MOZART-4 in the Arctic**

307 To assess the capacity of a model to estimate columns and variabilities of tropospheric species in  
308 the high Arctic, MOZART-4 was compared to the FTIR datasets. First, the general agreement  
309 between MOZART-4 and the measurements from 2008 to 2012 is discussed. Then we focus on  
310 2008 to analyze the model's ability to reproduce the different seasonal cycles of the seven target  
311 species in the troposphere. Finally, we focus on the most extreme fire event detected in our  
312 measurements in August-October 2010, to discuss biomass burning emissions used in the model.

### 313 **3.2.1) General comparisons between MOZART-4 and the FTIR datasets**

314 For comparisons with the FTIR datasets, all MOZART-4 data within the closest grid box to both  
315 measurement sites, and within three hours of each FTIR measurement are selected. The FTIR and  
316 the MOZART-4 trace gas profiles are estimated over different altitude ranges, and with different  
317 vertical resolutions. For each molecule, the MOZART-4 profiles are combined with FTIR *a priori*  
318 profiles between 1.9 hPa (~ 31 km) and 120 km. After extrapolating these model profiles onto the  
319 FTIR pressure grid, the model profiles are smoothed by convolution with the FTIR averaging

320 kernels functions (corresponding to that specific measurements) following the equation (Rodgers  
321 and Connors, 2003):

$$322 \quad \mathbf{x}_s = \mathbf{A}(\mathbf{x} - \mathbf{x}_a) + \mathbf{x}_a \quad (1)$$

323 where  $\mathbf{x}_s$  is the smoothed MOZART-4 profile,  $\mathbf{A}$  is the FTIR averaging kernel matrix and  $\mathbf{x}_a$  is the  
324 FTIR *a priori* profile. Then, total and tropospheric partial columns (between 0 and 10.25 km) are  
325 recalculated from the smoothed model profiles. Typical FTIR averaging kernels of the seven  
326 tropospheric can be seen in Viatte et al. (2014).

327 The FTIR retrievals have different vertical sensitivities for each species, characterized by the  
328 Degrees Of Freedom for Signal (DOFS), ranging on average over 4454 and 1747 measurements  
329 from 2.6 to 0.9 for CO and H<sub>2</sub>CO at Eureka, respectively. For comparisons with the model, total  
330 or partial columns may be considered, given the DOFS for that species. For CO, HCN, and C<sub>2</sub>H<sub>6</sub>,  
331 DOFS can be used to separate tropospheric columns from stratospheric columns, therefore  
332 tropospheric partial columns are considered in the comparison with the MOZART-4 data. For the  
333 others (C<sub>2</sub>H<sub>2</sub>, CH<sub>3</sub>OH, HCOOH, and H<sub>2</sub>CO), the average DOFS are on order unity, therefore only  
334 total columns are considered. However, these FTIR total columns that are the integrated abundance  
335 from the surface to 120 km, are representative of the partial columns (0-30 km) because the FTIR  
336 retrievals of these troposphere species have almost no sensitivity above 30 km, and the  
337 tropospheric columns represent more than 90% of the total columns (Viatte et al., 2014).

338 The results of comparing the MOZART-4 model and FTIR measurements over selected periods  
339 from 2008-2012 are shown in Tables 3 and 4, for Eureka and Thule, respectively. N is the number  
340 of measurements included in the comparison with MOZART-4. The coefficient of linear  
341 correlation (r) ranges from 0.35 to 0.93, where only two are less than 0.5 and the mean is 0.73.  
342 This shows strong correlations between the model and the measurements despite the larger size of  
343 MOZART-4 box (1.9°x2.5°) compared to our column measurements. Excellent correlations are  
344 found for CO, C<sub>2</sub>H<sub>6</sub>, and C<sub>2</sub>H<sub>2</sub>, for which  $r > 0.74$  at both sites, confirming that the model explains  
345 at least 54% of the atmospheric variability of these species in the Arctic. For HCN, the correlation  
346 is better at Eureka ( $r = 0.92$ ) than at Thule ( $r = 0.55$ ), however the relative differences between the  
347 model and the measurements are small ( $6.7 \pm 19.3$  % for Eureka and  $2.2 \pm 19.5$  % for Thule),  
348 highlighting the very good agreements between these datasets. Also, strong correlations are found  
349 for CH<sub>3</sub>OH ( $r = 0.77$  for Eureka and 0.62 for Thule). For HCOOH and H<sub>2</sub>CO, the correlations of  
350 0.60 and 0.50, and 0.35 and 0.75, for Eureka and Thule respectively, confirm the difficulty in

351 modelling the concentrations of these short-lived species in the high Arctic, and highlight the  
352 relatively poor understanding of the sources and sinks of these two molecules.

353 The mean relative differences  $((\text{model-FTIR})/\text{model})$  between MOZART-4 and CO and HCN  
354 partial columns are  $-2.9 \pm 7.5\%$  and  $6.7 \pm 19.3\%$  for Eureka, and  $-2.5 \pm 11.4\%$  and  $2.2 \pm 19.4\%$   
355 for Thule, respectively. The one-sigma standard deviations are larger than the means, confirming  
356 the agreement between the model data and the FTIR observations. For C<sub>2</sub>H<sub>6</sub> partial columns, the  
357 mean relative differences of  $-50.3 \pm 22.7\%$  and  $-54.1 \pm 29.7\%$  for Eureka and Thule, respectively,  
358 are higher than the standard deviations. We infer that there is a significant underestimation of the  
359 C<sub>2</sub>H<sub>6</sub> concentrations calculated by the model compared to the FTIR measurements. Our results  
360 confirm the underestimation of the model already highlighted with aircraft measurements during  
361 the ARCTAS campaign (Tilmes et al., 2011; Emmons et al., 2014). The CH<sub>3</sub>OH mean relative  
362 differences of  $-23.3 \pm 23.4\%$  and  $1.9 \pm 40.8\%$  for Eureka and Thule respectively, show good  
363 agreement between MOZART-4 and the CH<sub>3</sub>OH FTIR total columns, especially when considering  
364 the error bars of the measurements ( $\sim 12\%$ ). For C<sub>2</sub>H<sub>2</sub> and H<sub>2</sub>CO total columns, the agreements are  
365 poor with large standard deviations, and for HCOOH, the model did not include biogenic  
366 emissions, explaining the extreme differences.

367 Finally, the slopes (model vs. FTIR) are all less than one except for C<sub>2</sub>H<sub>2</sub>. This indicates that the  
368 model underestimates the columns relative to the FTIR data, suggesting that the model  
369 underestimates either emissions or transport of the seven tropospheric species in the high Arctic.  
370 It could also suggest that the model overestimates their chemical destructions in smoke plumes  
371 because of reduced photochemical activity due to aerosol scattering.

### 372 **3.2.2) Comparisons of the FTIR and MOZART-4 seasonal cycles in 2008**

373 The 2008 timeseries of daily mean CO, HCN, C<sub>2</sub>H<sub>6</sub>, C<sub>2</sub>H<sub>2</sub>, CH<sub>3</sub>OH, and H<sub>2</sub>CO total columns  
374 measured by the FTIRs at Eureka and Thule (Figure 5, blue and green dots, respectively), and  
375 calculated by MOZART-4 at these two sites (Figure 5, black and red dashed lines, respectively)  
376 are used to compare their seasonal cycles. This year was chosen because the April and July biomass  
377 burning events have been studied during the ARCTAS campaign (Jacob et al., 2010 and references  
378 therein). There are no CH<sub>3</sub>OH measurements at Thule for 2008, because the optical filter used to  
379 measure this gas was installed in 2010. HCOOH timeseries are excluded here, because the  
380 MOZART-4 runs did not include online biogenic emissions, which have been shown to be a large

381 source of HCOOH from the boreal forest (Stavrakou et al., 2012), and therefore the model does  
382 not capture HCOOH concentrations and variabilities, by at least an order of magnitude.

383 In winter, CO and C<sub>2</sub>H<sub>2</sub> total columns estimated by MOZART-4 agree very well with the FTIR  
384 measurements, suggesting that transport is well represented in the model, since it is the major  
385 process controlling the Arctic budget of these long-lived gases in winter. However, for C<sub>2</sub>H<sub>6</sub> which  
386 is also a long-lived tracer, the underestimation of its concentrations by MOZART-4 in winter  
387 confirms an underestimation in anthropogenic emissions in the model. For HCN, the good  
388 agreement in winter also confirms that transport is well reproduced in the model since HCN is the  
389 longest lived species of those studied here (five months in the troposphere, Li et al., 2003). In  
390 spring and summer, however, the overestimation of the model concentrations suggest that loss  
391 processes for HCN are missing, confirming that its sinks are not well quantified (Zeng et al., 2012).  
392 The CH<sub>3</sub>OH seasonal cycle estimated by MOZART-4 exhibits the best agreement with the  
393 observational datasets at Eureka.

394 Focusing on the July 2008 biomass burning event, the CH<sub>3</sub>OH enhanced concentrations are well  
395 captured by the model, suggesting that its fire emissions are correct. For CO and H<sub>2</sub>CO,  
396 enhancements estimated by the model are too low compared to the measurements. This might  
397 indicate that their fire emissions are too low in the model. In contrast, the modelled and measured  
398 HCN enhancements are similar, so fire emissions of HCN in the model seem appropriate. For C<sub>2</sub>H<sub>6</sub>  
399 and C<sub>2</sub>H<sub>2</sub>, the modelled enhancements are extremely low compared to the measurements,  
400 indicating missing sources.

### 401 **3.2.3 Comparisons of MOZART-4 and FTIR during the August 2010 fire events**

402 To further assess the estimation of fire emissions in the model, we focus on the most extreme event  
403 in our datasets in August 2010. Details about origin and transport of the plume from Russia through  
404 the Arctic are described in Viatte et al. (2013). Figure 6 shows the timeseries of CO, HCN, C<sub>2</sub>H<sub>6</sub>,  
405 C<sub>2</sub>H<sub>2</sub>, CH<sub>3</sub>OH, and H<sub>2</sub>CO total columns measured by the FTIR at Eureka (blue dots) and Thule  
406 (green dots) and calculated by MOZART-4 at Eureka (black dashed line) and Thule (red dashed  
407 line) for the August 2010 fire event.

408 Except for C<sub>2</sub>H<sub>6</sub> and C<sub>2</sub>H<sub>2</sub>, total columns measured by the FTIR and calculated by the model are  
409 generally in agreement during this fire event. In addition, enhancements due to the fire plume  
410 recorded at both stations around August 23<sup>rd</sup>, are captured in the model. However, the amplitudes

411 of these enhancements in MOZART-4, which reflect fire emissions in the model, seem too low for  
412 all the gases, except for CH<sub>3</sub>OH and H<sub>2</sub>CO. For CO, fire emissions in MOZART-4 are too low, as  
413 seen previously (Section 3.2.2). For C<sub>2</sub>H<sub>6</sub> and C<sub>2</sub>H<sub>2</sub>, concentrations calculated by the model are  
414 biased low, indicating missing sources. For CH<sub>3</sub>OH, fire emissions estimated in the model seem  
415 appropriate.

### 416 **3.3) Estimation of emissions from fires with FTIR measurements**

#### 417 **3.3.1) Correlation between CO and the other trace gases**

418 In order to estimate emissions from fires, all fire-affected measurements identified in the biomass  
419 burning events reaching the two Arctic sites (Tables 5 and 6) from 2008 to 2012, are used.  
420 Concentrations within smoke plumes vary rapidly with time, so emission factors are derived by  
421 measuring the emission ratio of the target chemical species relative to a reference species, which  
422 is often CO<sub>2</sub> or CO (Hurst et al., 1994). We use CO as the reference because these measurements  
423 are most sensitive to plume enhancements. Because the emission ratio is not measured at the source  
424 of the fire, the down-stream measurements here more accurately yield an “Enhancement Ratio”  
425 (EnhR). These ratios are derived from the regression slopes of a given trace gas total column versus  
426 that of CO, for each fire event. Since the spectral acquisitions require the use of optical filters and  
427 spectra are taken sequentially, we selected all CO measurements made within a 20-minute interval  
428 of the target gas measurement in order to calculate enhancement ratios. **Uncertainties on this  
429 tracer/tracer enhancement ratios method are small if both tracers have long atmospheric lifetimes  
430 relative to plume travel durations between the fire source and the measurements. In addition, errors  
431 on transport and plume altitude are also minimized since all tracers are expected to be mixed and  
432 transported in the same airmasses. These assumptions constitute the main limitation of this  
433 approach (Yokelson et al., 2013).**

434 Figure 7 and 8 show the correlation plots of the total columns of the target species relative to CO,  
435 for all fire events (represented by different colors) detected at Eureka and Thule, respectively. For  
436 Eureka (and Thule), the enhancement ratios are estimated from each biomass burning event, with  
437 313 (136), 321 (274), 205 (137), 228 (-), 202 (120), and 298 (149) pairs of CO columns with HCN,  
438 C<sub>2</sub>H<sub>6</sub>, C<sub>2</sub>H<sub>2</sub>, CH<sub>3</sub>OH, HCOOH, and H<sub>2</sub>CO columns, respectively. Given the small number of  
439 CH<sub>3</sub>OH FTIR observations at Thule, we did not estimate its enhancement ratio here (see below).

440 The correlations of HCN, CH<sub>3</sub>OH, HCOOH, and H<sub>2</sub>CO total columns with CO using all of the fire  
441 datasets (all colors combined, Figure 7 and 8) are not linear, since these species have different  
442 atmospheric lifetimes from CO (Viatte et al., 2014). In contrast, CO, C<sub>2</sub>H<sub>6</sub>, and C<sub>2</sub>H<sub>2</sub> have common  
443 sinks and sources, so their columns are expected to be correlated throughout the year. Except for  
444 H<sub>2</sub>CO, correlations of the fire species with CO in the individual fire plumes (individual colors,  
445 Figure 7 and 8) exhibit linear patterns. This confirms that the target gases are transported in the  
446 same airmasses from the emitted fire sources. For H<sub>2</sub>CO, the correlations with CO are not clearly  
447 linear inside fire plumes. However, the measured total columns are significantly enhanced (up to  
448  $4.5 \times 10^{15}$  molecules/cm<sup>2</sup>) in August 2008 at Thule, in August and July 2010 at Eureka and Thule,  
449 respectively, in June 2011 and July 2011 at both sites, as well as in July 2012 at Thule. Given the  
450 back-trajectory analyses, these enhanced H<sub>2</sub>CO columns recorded in the high Arctic are correlated  
451 with extreme fire events in the boreal forest during summer.

452 For each event, the slopes of the regression lines are taken as the enhancement ratios of the species  
453 emitted by fires. **The correlations are obtained by linear regression using the method of York et al.**  
454 **(2004), which takes into account uncertainties in both ordinate and abscissa variables. The total**  
455 **uncertainty for the regression slopes is calculated by quadrature addition of the fit uncertainties**  
456 **and the measurement uncertainties.** Those values are summarized in Tables 5 and 6 for Eureka and  
457 Thule, respectively. N is the number of pairs (between the target species vs. CO) used to estimate  
458 the enhancement ratios, r is the correlation coefficient of the linear regression, 'EnhR' is the  
459 enhancement ratios given by the slope of the regression line for each fire event. **To assess changes**  
460 **due to photochemistry during plume aging (Akagi et al., 2012), the enhancement ratios corrected**  
461 **by the travel time of the plume ('ER') have been included in Tables 5 and 6.** If less than six pairs  
462 are measured in a fire plume, the enhancement ratios are not estimated from this event, i.e., C<sub>2</sub>H<sub>2</sub>  
463 measurements at Eureka in July 2010. No error weighting were performed according to the number  
464 of points.

465 The correlation coefficients between HCN and CO total columns are on average 0.84 and 0.79 for  
466 the Eureka and Thule datasets, respectively (last columns in Tables 5 and 6). Good correlations  
467 between C<sub>2</sub>H<sub>6</sub> and CO total columns (r = 0.81 on average for both datasets) also confirm that the  
468 selected measurements, listed in Tables 1 and 2, were made inside fire plumes. The mean of the  
469 correlation coefficients between C<sub>2</sub>H<sub>2</sub> and CO total columns inside plumes are 0.78 and 0.80, for  
470 Eureka and Thule respectively. For CH<sub>3</sub>OH, the average of the coefficients of correlation is 0.65  
471 at Eureka. The HCOOH total columns are also well correlated with CO inside the plumes, given

472 the average values of  $r$  of 0.79 and 0.58 at Eureka and Thule, respectively. However, the July 2010  
473 event has a negative correlation coefficient between HCOOH and CO at Thule, but the small  
474 numbers of points ( $N = 6$  and  $8$ , for Eureka and Thule, respectively) are too low to draw significant  
475 conclusions. The mean correlation coefficients between H<sub>2</sub>CO and CO total columns are similar:  
476  $r = 0.41$  and  $0.40$  at Eureka and Thule, respectively. Given the short atmospheric lifetime of this  
477 molecule and the fact that the measurements are not performed at the source of the fires, H<sub>2</sub>CO  
478 could have been destroyed in the atmosphere while transported through the Arctic. However, the  
479 wide ranges of the  $r$  values, from 0.08 to 0.90 at Eureka in March 2008 and July 2012, and from  
480 0.34 to 0.93 in August 2008 and June 2011 at Thule, suggest a possible secondary production of  
481 H<sub>2</sub>CO in some atmospheric smoke plumes, where  $r$  is high. Young and Paton-Walsh (2011) also  
482 show that concentrations of H<sub>2</sub>CO within Australian smoke plumes increase during the first day  
483 of travel before declining two days after they were emitted.

484 The enhancement ratios are expected to vary with the travel time of the plumes from their source  
485 to the measurement site (see last columns in Tables 1 and 2), especially for short-lived species  
486 because of their faster atmospheric destruction (via photochemistry, oxidation, as well as dry and  
487 wet depositions) compared to CO. However, the mean enhancement ratios of the target gases over  
488 all fire events are comparable for the two sites. For instance, the Eureka and Thule mean  
489 enhancement ratios of HCN, over all biomass burning events, are  $0.00334 \pm 0.00094$  (one-sigma  
490 standard deviation) and  $0.00429 \pm 0.00245$ , respectively (last columns in Tables 5 and 6). In  
491 addition, the enhancements ratios of HCN, C<sub>2</sub>H<sub>6</sub>, and C<sub>2</sub>H<sub>2</sub> estimated from the extreme fire event  
492 of August 2010 are very similar:  $0.00563$  and  $0.00650$  for HCN,  $0.01019$  and  $0.01235$  for C<sub>2</sub>H<sub>6</sub>,  
493  $0.00189$  and  $0.00191$  for C<sub>2</sub>H<sub>2</sub>, for Eureka and Thule, respectively.

### 494 **3.3.2) Calculation of Emission Ratios (ER) and Emission Factors (EF)**

495 In models, fire emissions are often specified by using emission ratios relative to a reference  
496 species, typically CO, which correspond to measured ratios at the source of the biomass burning  
497 event. Those emission ratios are equal to the enhancement ratios corrected for the travel duration  
498 of the plume. By considering the different lifetimes of the molecules (Table 3, last column) as well  
499 as the plume travel times to reach Eureka and Thule (last columns of Tables 1 and 2), we calculated  
500 the decay rates of each species to obtain the percentage of their initial values remaining when they  
501 were measured. This allows the measured enhancement ratios to be corrected to the equivalent  
502 emission ratios (Paton-Walsh et al., 2005; Akagi et al., 2011; Hornbrook et al., 2011). More details

503 regarding this correction are found in Viatte et al. (2013). Since the uncertainty in the correction  
504 is small compared to other uncertainties, our equivalent emission ratios can be compared to other  
505 emission ratios found in the literature. For comparison with previous studies, our equivalent  
506 emission ratios have been converted into equivalent emission factors using (Andreae and Merlet,  
507 2001):

$$508 \quad EF_x = ER_{(x/CO)} \times (MW_x/MW_{CO}) \times EF_{CO} \quad (2)$$

509 where  $EF_x$  is the emission factor for trace gas X in grams of gas per kg of dry biomass burnt;  
510  $ER_{(x/CO)}$  is the molar emission ratio of trace gas X with respect to CO;  $MW_x$  is the molecular weight  
511 of trace gas X;  $MW_{CO}$  is the molecular weight of CO, and  $EF_{CO}$  is the emission factor of CO.

512 In this study, values of  $EF_{CO}$  of  $127 \pm 45 \text{ g kg}^{-1}$  and  $107 \pm 37 \text{ g kg}^{-1}$  for dry matter based on Akagi et  
513 al. (2011) and Andreae and Merlet (2001), respectively, are taken as the emission factor for CO  
514 for boreal and extratropical forests, since this is the fuel type of the relevant source fires (vegetation  
515 type columns in Tables 1 and 2). Uncertainties in the measured EF are calculated by taking into  
516 account the large uncertainty in the CO emission factor (more than 35%) and the uncertainty in  
517 the mean calculated regression slope (33.6%, 54.0%, 49.5%, 32.2% and 22.8% for HCN, C<sub>2</sub>H<sub>6</sub>,  
518 C<sub>2</sub>H<sub>2</sub>, CH<sub>3</sub>OH, and HCOOH at Eureka respectively, and 43.5%, 33.1%, 52.5%, and 16.3% for  
519 HCN, C<sub>2</sub>H<sub>6</sub>, C<sub>2</sub>H<sub>2</sub>, and HCOOH respectively, at Thule), as well as the total uncertainties of the  
520 retrievals (3.1%, 10.5%, 14.3%, 22.5%, 12.3%, and 17.0% for CO, HCN, C<sub>2</sub>H<sub>2</sub>, C<sub>2</sub>H<sub>6</sub>, CH<sub>3</sub>OH,  
521 and HCOOH, respectively; Viatte et al., 2014, their Table 3), all combined in quadrature (Paton-  
522 Walsh et al., 2005). Total uncertainties on EF are 49.2%, 67.3%, 61.8%, 48.7%, and 42.3% for  
523 HCN, C<sub>2</sub>H<sub>6</sub>, C<sub>2</sub>H<sub>2</sub>, CH<sub>3</sub>OH, and HCOOH, at Eureka respectively, and 57.5%, 48.7%, 63.8%, and  
524 46.5% for HCN, C<sub>2</sub>H<sub>6</sub>, C<sub>2</sub>H<sub>2</sub>, and HCOOH, at Thule respectively. Because the uncertainties on the  
525 FTIR H<sub>2</sub>CO retrievals are high (~27 %) and the transport times of the plumes to the Arctic exceed  
526 its atmospheric lifetime (which is less than two days), emission ratios of H<sub>2</sub>CO have not been  
527 estimated in this study.

528 Our corrected enhancement ratios (i.e., equivalent emission ratios, 'ER' in Tables 5 and 6) have  
529 been converted into equivalent emission factors using Equation 2. Only enhancement ratios  
530 calculated from more than 6 pairs ( $N > 6$ ), and satisfying a coefficient of correlation of more than  
531 0.6 ( $r > 0.6$ ) are taken into account to estimate emission factors. The means of equivalent emission  
532 ratios and emission factors (calculated using  $EF_{CO}$  for the extratropical forest) estimated from  
533 FTIR measurements performed at Eureka and Thule are summarized in Table 7.

534 Figure 9 shows the emission factors calculated from FTIR measurements performed at Eureka  
535 (cyan) and Thule (green), using the same  $EF_{CO}$  of Andreae and Merlet (2001) for the extratropical  
536 forest. All emission factors estimated from both FTIR datasets agree well within combined error  
537 bars. The mean of the emission factors estimated from the Eureka and Thule FTIR datasets are  
538  $0.36 \pm 0.17 \text{ g kg}^{-1}$  and  $0.44 \pm 0.25 \text{ g kg}^{-1}$  for HCN,  $1.09 \pm 0.74 \text{ g kg}^{-1}$  and  $1.39 \pm 0.68 \text{ g kg}^{-1}$  for  
539  $C_2H_6$ ,  $0.40 \pm 0.25 \text{ g kg}^{-1}$  and  $0.28 \pm 0.18 \text{ g kg}^{-1}$  for  $C_2H_2$ , and  $2.69 \pm 1.14 \text{ g kg}^{-1}$  and  $3.15 \pm 1.46 \text{ g}$   
540  $\text{kg}^{-1}$  for HCOOH, respectively. For  $CH_3OH$ , we estimated a mean emission factor of  $3.44 \pm 1.68$   
541  $\text{g kg}^{-1}$  at Eureka (Table 7). The emission factors derived from the Thule dataset are slightly higher  
542 than those for Eureka, except for  $C_2H_2$ , but these differences are not significant given the error  
543 bars. However, the  $EF_{HCOOH}$  is notably higher at Thule than at Eureka. A possible explanation is  
544 that our Thule measurements of HCOOH from fire events are contaminated by local biogenic  
545 emissions.

546 In order to compare our results with others, emission factors from two compilations of data  
547 (Andreae and Merlet, 2001; Akagi et al., 2011) for extratropical and boreal forests have been  
548 selected. These studies contain a comprehensive set of emission factors from the burning of  
549 numerous vegetation types derived from various measurement platforms. Figure 10 shows the  
550 emission factors calculated from the FTIR measurements (in blue and cyan), along with the  
551 emission factors found in the compilation studies of Akagi et al. (2011) (red) and Andreae and  
552 Merlet (2001) (pink). The blue colour corresponds to the emission factors calculated using the  
553  $EF_{CO}$  for the boreal forest from Akagi et al. (2011), whereas the cyan colours corresponds to the  
554 values of  $EF_x$  calculated using the  $EF_{CO}$  for the extratropical forest from Andreae and Merlet  
555 (2001).

556 Our  $EF_{HCN}$  are lower than the two mean values reported in the literature. The sources and sinks of  
557 HCN are not well known. Our  $EF_{C_2H_6}$  agree well, within combined error, with the mean value  
558 reported by Akagi et al. (2011) and are higher than the mean value reported in the earlier study of  
559 Andreae and Merlet (2001). The emission factors of  $C_2H_2$  estimated from the FTIR measurements  
560 are in excellent agreement with the mean values reported in both compilation studies. Our  $EF_{CH_3OH}$   
561 are in agreement with the mean value from Akagi et al. (2011) and are higher than the mean value  
562 reported by Andreae and Merlet (2001) suggesting that  $CH_3OH$  emissions from fires are higher  
563 than previously thought. Finally, our  $EF_{HCOOH}$  are significantly higher than the values reported in  
564 the more recent compilation study of Akagi et al. (2011), but agree well with the mean value  
565 reported in 2001 (Andreae and Merlet, 2001). This may suggest that fires from the extratropical

566 forest emit relatively large amount of HCOOH, or it may reflect a local biogenic component in our  
567 measurements.

#### 568 **4) Summary and conclusions**

569 The frequency and intensity of biomass burning are strongly linked to climate change, and  
570 constitute a large source of the variability in Arctic tropospheric composition. We performed FTIR  
571 measurements of seven important biomass burning species (CO, HCN, C<sub>2</sub>H<sub>6</sub>, C<sub>2</sub>H<sub>2</sub>, CH<sub>3</sub>OH,  
572 HCOOH, and H<sub>2</sub>CO) at two high Arctic sites, Eureka and Thule, from 2008 to 2012. We focused  
573 on these species for several reasons: (1) there remain numerous gaps in the available tropospheric  
574 observational datasets, especially at high latitudes. (2) Since these species exhibit different source  
575 fractions (anthropogenic, biogenic, fossil fuel burning, and biomass burning), as well as different  
576 lifetimes, the comparison of our new datasets with chemical transport model simulations can help  
577 identify issues in the model that can be addressed to improve their estimations of trace gas  
578 concentrations and temporal variations, as well as transport processes in the high Arctic. (3) All  
579 these biomass burning products are measured almost simultaneously using the FTIR technique, so  
580 we derived emission factors to add new values to the relatively sparse datasets in the literature.

581 Those new datasets of tropospheric species recorded at both stations exhibit similar seasonal  
582 cycles, in term of absolute values and temporal variabilities. In addition, ten and eight fire events  
583 were identified at Eureka and Thule, respectively. These highlight the importance of the biomass  
584 burning long-range transport in the Arctic budget of NMHC, which can affect air quality and  
585 climate in this region. This may have a continued and increasing effect in a warming climate and  
586 sensitive Arctic eco-system.

587 The two sets of measurements were compared with MOZART-4 to assess (1) the general  
588 agreement (2008-2012), (2) the model simulations of the different seasonal cycles (with the 2008  
589 year), and (3) fire emissions in the model. Correlations between MOZART-4 and FTIR total  
590 columns are strong (r ranges from 0.35 to 0.93). The mean relative differences between MOZART-  
591 4 and the CO and HCN measurements confirm the good agreement between the model data and  
592 the FTIR observations. In winter, CO and C<sub>2</sub>H<sub>2</sub> total columns estimated by MOZART-4 agree well  
593 with the FTIR measurements, suggesting that transport is well represented in the model, since it is  
594 the major process controlling the Arctic budget of these long tropospheric lifetime gases. However,  
595 for C<sub>2</sub>H<sub>6</sub> the low columns estimated in winter by MOZART-4 confirm an underestimation in its  
596 emissions in the model. For HCN, the good agreement in winter also confirms that transport is

597 well reproduced. In spring and summer, however, the overestimation of the model columns  
598 suggests that loss processes for HCN are missing. Finally, the CH<sub>3</sub>OH total columns show good  
599 agreement between MOZART-4 and the FTIR dataset at Eureka.

600 In order to estimate emissions from fires, all fire-affected spectra recorded inside smoke plumes  
601 were used to calculate the enhancement ratios relative to CO. Very good correlations with CO are  
602 found inside smoke plumes in the Arctic, confirming the common fire origins and transport  
603 pathways. CO and H<sub>2</sub>CO total columns are well correlated ( $r > 0.9$ ) inside fire plumes transported  
604 in June 2011 to Thule and in July 2012 to Eureka, suggesting a possible secondary production of  
605 H<sub>2</sub>CO in atmospheric smoke plumes. The enhancement ratios were used to derive equivalent  
606 emission ratios from which emission factors were calculated using an assumed emission factor for  
607 CO. The means of emission factors estimated with the two FTIR datasets are  $0.40 \pm 0.21 \text{ g kg}^{-1}$   
608 for HCN,  $1.24 \pm 0.71 \text{ g kg}^{-1}$  for C<sub>2</sub>H<sub>6</sub>,  $0.34 \pm 0.21 \text{ g kg}^{-1}$  for C<sub>2</sub>H<sub>2</sub>, and  $2.92 \pm 1.30 \text{ g kg}^{-1}$  for  
609 HCOOH. The emission factor for CH<sub>3</sub>OH estimated at Eureka is  $3.44 \pm 1.68$   
610  $\text{g kg}^{-1}$ . These measurements add new observations to the sparse dataset of emission factors that  
611 have been reported and compiled in the literature.

612 An extension of this work would be to compare the FTIR measurements to the CAM-chem model  
613 (Lamarque et al., 2010), which has online MEGAN biogenic emissions for many species, such as  
614 methanol and formic acid, to assess how this improves the comparison compared to MOZART-4.  
615

## 616 **Acknowledgments**

617 This work was supported by NSERC. The PEARL Bruker 125HR measurements at Eureka were  
618 made by CANDAC, which has been supported by the AIF/NSRIT, CFI, CFCAS, CSA, EC,  
619 Government of Canada IPY funding, NSERC, OIT, ORF, PCSP, and FQRNT. The authors wish  
620 to thank the staff at the Eureka Weather Station and CANDAC for the logistical and on-site support  
621 provided. Thanks to Rodica Lindenmaier, Rebecca Batchelor, PEARL Site Manager Pierre Fogal,  
622 and CANDAC/PEARL operators Ashley Harrett, Alexei Khmel, Paul Loewen, Keith MacQuarrie,  
623 Oleg Mikhailov, and Matt Okraszewski, for their invaluable assistance in maintaining the Bruker  
624 125HR and for taking measurements. The National Center for Atmospheric Research is supported  
625 by the National Science Foundation. The observation program at Thule, GR is supported under  
626 contract by the National Aeronautics and Space Administration and the site is also supported by  
627 the NSF Office of Polar Programs. We wish to thank the Danish Meteorological Institute for

628 support at the Thule. The authors also acknowledge NOAA-ARL for access to the HYSPLIT  
629 trajectory model, and NASA for its MODIS and OMI imagery products available from their  
630 Rapidfire website and from the Giovanni online data system, developed and maintained by the  
631 NASA GES DISC. The visit of C. Paton-Walsh to the UofT to collaborate on this study was funded  
632 by the ARC as part of the project DP110101948.

633 **References:**

634 Andreae, M. O., and Merlet, P.: Emission of trace gases and aerosols from biomass burning, *Global*  
635 *Biogeochem. Cy.*, 15, 955–966, doi:10.1029/2000GB001382, 2001.

636 Akagi, S. K., Yokelson, R. J., Wiedinmyer, C., Alvarado, M. J., Reid, J. S., Karl, T., Crounse, J.  
637 D., and Wennberg, P. O.: Emission factors for open and domestic biomass burning for use in  
638 atmospheric models, *Atmos. Chem. Phys.*, 11, 4039–4072, doi:10.5194/acp-11-4039-2011, 2011.

639 Akagi, S. K., Craven, J. S., Taylor, J. W., McMeeking, G. R., Yokelson, R. J., Burling, I. R.,  
640 Urbanski, S. P., Wold, C. E., Seinfeld, J. H., Coe, H., Alvarado, M. J., and Weise, D. R.: Evolution  
641 of trace gases and particles emitted by a chaparral fire in California, *Atmos. Chem. Phys.*, 12,  
642 1397–1421, doi:10.5194/acp-12-1397-2012, 2012.

643 Amiro, B.D., Cantin, A., Flannigan, M.D. and de Groot, W.J.: Future emissions from Canadian  
644 boreal forest fires, *Can. J. For. Res.*, 39, 383–395, doi: 10.1139/X08-154, 2009.

645 Barrett, C., Kelly, R., Higuera, P. E., and Hu, F.S.: Climatic and land-cover influences on the  
646 spatiotemporal dynamics of Holocene boreal fire regimes, *Ecology*, 94, 389–402,  
647 <http://dx.doi.org/10.1890/12-0840.1>, 2013.

648 Bian, H., Colarco, P. R., Chin, M., Chen, G., Rodriguez, J. M., Liang, Q., Blake, D., Chu,  
649 D. A., da Silva, A., Darmenov, A. S., Diskin, G., Fuelberg, H. E., Huey, G., Kondo, Y., Nielsen,  
650 J. E., Pan, X., and Wisthaler, A.: Source attributions of pollution to the Western Arctic during the  
651 NASA ARCTAS field campaign, *Atmos. Chem. Phys.*, 13, 4707–4721, doi:10.5194/acp-13-4707-  
652 2013, 2013.

653 Coffey, M. T., Goldman, A., Hannigan, J. W., Mankin, W. G., Schoenfeld, W. G., Rinsland, C. P.,  
654 Bernardo, C., and Griffith, D. W. T.: Improved vibration-rotation (0-1) HBr line parameters for  
655 validating high resolution infrared atmospheric spectra measurements, *J. Quant. Spectrosc. Radiat.*  
656 *Transf.*, 60, 863–867, doi:10.1016/S0022-4073(98)00088-0, 1998.

657 Coheur, P.-F., Herbin, H., Clerbaux, C., Hurtmans, D., Wespes, C., Carleer, M., Turquety, S., P.  
658 Rinsland, C. P., Remedios, J., Hauglustaine, D., Boone, C. D., and Bernath, P. F.: ACE-FTS  
659 observation of a young biomass burning plume: first reported measurements of C<sub>2</sub>H<sub>4</sub>, C<sub>3</sub>H<sub>6</sub>O,  
660 H<sub>2</sub>CO and PAN by infrared occultation from space, *Atmos. Chem. Phys.*, 7, 5437–5446,  
661 doi:10.5194/acp-7-5437-2007, 2007.

662 Coheur, P.-F., L. Clarisse, S. Turquety, D. Hurtmans, *and* C. Clerbaux IASI measurements of  
663 reactive trace species in biomass burning plumes, *Atmos. Chem. Phys.*, *9*, 5655–5667,  
664 doi:10.5194/acp-9-5655-2009, 2009.

665 Colarco, P. R., Schoeberl, M. R., Doddridge, B. G., Marufu, L. T., Torres, O., and Welton, E. J.:  
666 Transport of smoke from Canadian forest fires to the surface near Washington, D.C.: Injection  
667 height, entrainment, and optical properties, *J. Geophys. Res.*, *109*(D6), D06203, doi:  
668 10.1029/2003JD004248, 2004.

669 Daniel, J. S., and Solomon, S.: On the climate forcing of carbon monoxide, *J. Geophys. Res.*,  
670 *103*(D11), 13249–13260, doi:10.1029/98JD00822, 1998.

671 Eyring, V., Waugh, D. W., Bodeker, G. E., Cordero, E., Akiyoshi, H., Austin, J., Beagley, S. R.,  
672 Boville, B. A., Braesicke, P., Brühl, C., Butchart, N., Chipperfield, M. P., Dameris, M., Deckert,  
673 R., Deushi, M., Frith, S. M., Garcia, R. R., Gettelman, A., Giorgetta, M. A., Kinnison, D. E.,  
674 Mancini, E., Manzini, E., Marsh, D. R., Matthes, S., Nagashima, T., Newman, P. A., Nielsen, J.  
675 E., Pawson, S., Pitari, G., Plummer, D. A., Rozanov, E., Schraner, M., Scinocca, J. F., Semeniuk,  
676 K., Shepherd, T. G., Shibata, K., Steil, B., Stolarski, R. S., Tian W., and Yoshiki, M.: Multi-model  
677 projections of stratospheric ozone in the 21st century, *J. Geophys. Res.*, *112*, D16303,  
678 doi:10.1029/2006JD008332, 2007.

679 Eckhardt, S., Stohl, A., Beirle, S., Spichtinger, N., James, P., Forster, C., Junker, C., Wagner, T.,  
680 Platt, U., and Jennings, S. G.: The North Atlantic Oscillation controls air pollution transport to the  
681 Arctic, *Atmos. Chem. Phys.*, *3*, 1769–1778, doi:10.5194/acp-3-1769-2003, 2003.

682 Emmons, L. K., Arnold S., Monks S., Huijnen V., Tilmes S., Law K., Thomas J. L., Raut J.-C.,  
683 Bouarar I., Turquety S., Long Y., Duncan B., Steenrod S., Strode S., Flemming J., Mao J., Langner  
684 J., Thompson A. M., Tarasick D., Apel E., Blake D., Brune W., Cohen R. C., Dibb J., Diskin G.  
685 S., Fried A., Hall S., Huey G., Weinheimer A. J., Wennberg P., Wisthaler A., Mikoviny T., de  
686 Gouw J., Holloway J., Montzka S., Nowak J., Peischl J., Roberts J., Ryerson T., Warneke C., and  
687 Helmig D.: The POLARCAT Model Intercomparison Project (POLMIP): Overview and  
688 evaluation with observations, *Atmos. Chem. Phys. Discuss.*, *14*, 29331–29393, doi:10.5194/acpd-  
689 14-29331-2014, 2014.

690 Emmons, L. K., Walters, S., Hess, P. G., Lamarque, J.-F., Pfister, G. G., Fillmore, D., Granier, C.,  
691 Guenther, A., Kinnison, D., Laepple, T., Orlando, J., Tie, X., Tyndall, G., Wiedinmyer, C.,

692 Baughcum, S. L., and Kloster, S.: Description and evaluation of the Model for Ozone and Related  
693 chemical Tracers, version 4 (MOZART-4), *Geosci. Model Dev.*, 3, 43–67, doi:10.5194/gmd-3-43-  
694 2010, 2010.

695 Finch, D. P., Palmer, P. I., and Parrington, M.: Origin, variability and age of biomass burning  
696 plumes intercepted during BORTAS-B: evidence for retardation of plume photochemistry, *Atmos.*  
697 *Chem. Phys. Discuss.*, 14, 8723–8752, doi:10.5194/acpd-14-8723-2014, 2014.

698 Fisher, J. A., Jacob, D. J., Purdy, M. T., Kopacz, M., Le Sager, P., Carouge, C., Holmes, C. D.,  
699 Yantosca, R. M., Batchelor, R. L., Strong, K., Diskin, G. S., Fuelberg, H. E., Holloway, J. S.,  
700 Hyer, E. J., McMillan, W. W., Warner, J., Streets, D. G., Zhang, Q., Wang, Y., and Wu, S.: Source  
701 attribution and interannual variability of Arctic pollution in spring constrained by aircraft  
702 (ARCTAS, ARCPAC) and satellite (AIRS) observations of carbon monoxide, *Atmos. Chem.*  
703 *Phys.*, 10, 977–996, doi:10.5194/acp-10-977-2010, 2010.

704 Flannigan, M., Stocks, B., Turetsky, M., and Wotton, M.: Impacts of climate change on fire activity  
705 and fire management in the circumboreal forest, *Glob. Change Biol.*, 15, 549–60, doi:  
706 10.1111/j.1365-2486.2008.01660.x, 2009.

707 Fogal, P. F., LeBlanc, L. M., and Drummond, J. R.: The Polar Environment Atmospheric Research  
708 Laboratory (PEARL): Sounding the Atmosphere at 80° North, *Arctic*, 66 (3), 377–386,  
709 doi:10.1175/2009JTECHA1215.1, 2013.

710 Garcia, R.R., Marsh, D. R., Kinnison, D. E., Boville, B. A., and Sassi, F.: Simulation of secular  
711 trends in the middle atmosphere, 1950–2003, *J. Geophys. Res.*, 112, D09301,  
712 doi:10.1029/2006JD007485, 2007.

713 Generoso, S., Breon, F., Chevallier, F., Balkanski, Y., Schulz, M., and Bey, I.: Assimilation of  
714 POLDER aerosol optical thickness into the LMDz-INCA model: Implications for the Arctic  
715 aerosol burden, *J. Geophys. Res.*, 112, D02311, doi: 10.1029/2005JD006954. issn: 0148–0227,  
716 2007.

717 Gerbig, C., Lin, J. C., Wofsy, S. C., Daube, B. C., Andrews, A. E., Stephens, B. B., Bakwin, P. S.,  
718 and Grainger, C. A.: Toward constraining regional-scale fluxes of CO<sub>2</sub> with atmospheric  
719 observations over a continent: 2. Analysis of COBRA data using a receptor-oriented framework,  
720 *J. Geophys. Res.-Atmos.*, 108, D24, 4757, doi:10.1029/2003JD003770, 2003.

721 Goldman, A., Paton-Walsh, C., Bell, W., Toon, G. C., Blavier, J. F., Sen, B., Coffey, M. T.,  
722 Hannigan, J. W., and Mankin, W. G.: Network for the detection of stratospheric change Fourier  
723 transform infrared intercomparison at Table Mountain Facility, *J. Geophys. Res.*, 104, 30481–  
724 30503, DOI: 10.1029/1999JD900879, 1999.

725 Hannigan, J. W., Coffey, M. T., Goldman, A.: Semiautonomous FTS Observation System for  
726 Remote Sensing of Stratospheric and Tropospheric Gases, *J. Atmos. Oceanic Technol.*, 26, 1814–  
727 1828, <http://dx.doi.org/10.1175/2009JTECHA1230.1>, 2009.

728 Hecobian, A., Liu, Z., Hennigan, C. J., Huey, L. G., Jimenez, J. L., Cubison, M. J., Vay, S., Diskin,  
729 G. S., Sachse, G. W., Wisthaler, A., Mikoviny, T., Weinheimer, A. J., Liao, J., Knapp, D. J.,  
730 Wennberg, P. O., Kürten, A., Crouse, J. D., St. Clair, J., Wang, Y., and Weber, R. J.: Comparison  
731 of chemical characteristics of 495 biomass burning plumes intercepted by the NASA DC-8 aircraft  
732 during the ARCTAS/CARB-2008 field campaign, *Atmos. Chem. Phys.*, 11, 13325–  
733 13337, doi:10.5194/acp-11-13325-2011, 2011.

734 Hornbrook, R. S., Blake, D. R., Diskin, G. S., Fried, A., Fuelberg, H. E., Meinardi, S., Mikoviny,  
735 T., Richter, D., Sachse, G. W., Vay, S. A., Walega, J., Weibring, P., Weinheimer, A. J.,  
736 Wiedinmyer, C., Wisthaler, A., Hills, A., Riemer, D. D., and Apel, E. C.: Observations of  
737 nonmethane organic compounds during ARCTAS - Part 1: Biomass burning emissions and plume  
738 enhancements, *Atmos. Chem. Phys.*, 11, 11103–11130, doi:10.5194/acp-11-11103-2011, 2011.

739 Hurst, D. F., Griffith, D. W. T., & Cook, G. D.: Trace gas emissions from biomass burning in  
740 tropical Australian savannas, *J. Geophys. Res.*, 99(D8), 16441–16456. doi:10.1029/94JD00670,  
741 1994.

742 IPCC: Climate Change 2007: The Physical Science Basis, edited by: Solomon, S., Quin, D.,  
743 Manning, M., Chen, Z., Marquis, M., Averyt, K. B., Tignor, M., and Miller, H. L., 500–657,  
744 Cambridge University Press, Cambridge, United Kingdom, USA, 2007.

745 Kasischke, E.S., and Turetsky, M.R.: Recent changes in the fire regime across the North American  
746 boreal region - Spatial and temporal patterns of burning across Canada and Alaska, *Geophys. Res.*  
747 *Let.*, 33, L09703, doi:10.1029/2006GL025677, 2006.

748 Kelly, R., Chipman, M. L., Higuera, P. E., Stefanov, I., Brubaker, L. B., and Hu, F. S.: Recent  
749 burning of boreal forests exceeds fire regime limits of the past 10,000 years, *PNAS*, 110, 13055–  
750 13060, doi:10.1073/pnas.1305069110, 2013.

751 Koch, D., and Hansen, J.: Distant origins of Arctic black carbon: A Goddard Institute for Space  
752 Studies Model experiment, *J. Geophys. Res.*, 110, D04204, doi:10.1029/2004JD005296, 2005.

753 Kurylo, M. J.: Network for the detection of stratospheric change (NDSC), *Proc. Soc. Photo-Opt.*  
754 *Instrum. Eng.*, 1491, 168–174, 1991.

755 Kurylo, M. J., and Zander R.: The NDSC – its status after 10 years of operation. Proceedings of  
756 the XIX Quadrennial Ozone Symposium, Hokkaido Univ., Sapporo, Japan on 3–8 July 2000, 167–  
757 168, 2000.

758 Lamarque, J.-F., Emmons, L. K., Hess, P. G., Kinnison, D. E., Tilmes, S., Vitt, F., Heald, C. L.,  
759 Holland, E. A., Lauritzen, P. H., Neu, J., Orlando, J. J., Rasch, P. J., and Tyndall, G. K.: CAM-  
760 chem: description and evaluation of interactive atmospheric chemistry in the Community Earth  
761 System Model, *Geosci. Model Dev.*, 5, 369-411, doi:10.5194/gmd-5-369-2012, 2012.

762 Le Breton, M., Bacak, A., Müller, J. B. A., O’Shea, S. J., Xiao, P., Ashfold, M. N. R., Cooke, M.  
763 C., Batt, R., Shallcross, D. E., Oram, D. E., Forster, G., Bauguitte, S. J.-B., and Percival, C. J.:  
764 Airborne HCN measurements from biomass burning, *Atmos. Chem. Phys.*, 13, 9217–9232,  
765 doi:10.5194/acp-13-9217-2013, 2013.

766 Lesins, G., Duck T. J., and Drummond, J. R.: Climate trends at Eureka in the Canadian high Arctic,  
767 *Atmosphere Ocean*, 48, 59–80, doi:10.3137/AO1103.2010, 2010.

768 Lewis, A. C., Evans, M. J., Hopkins, J. R., Punjabi, S., Read, K. A., Purvis, R. M., Andrews, S. J.,  
769 Moller, S. J., Carpenter, L. J., Lee, J. D., Rickard, A. R., Palmer, P. I., and Parrington, M.: The  
770 influence of biomass burning on the global distribution of selected non-methane organic  
771 compounds, *Atmos. Chem. Phys.*, 13, 851–867, doi:10.5194/acp-13-851-2013, 2013.

772 Li, Q., Jacob, D. J., Yantosca, R. M., Heald, C. L., Singh, H. B., Koike, M., Zhao, Y., Sachse, G.  
773 W., and Streets, D. G.: A global three-dimensional model analysis of the atmospheric budgets of  
774 HCN and CH<sub>3</sub>CN: Constraints from aircraft and ground measurements, *J. Geophys. Res.*,  
775 108(D21), 8827, doi:10.1029/2002JD003075, 2003.

776 Lin, J.C., Gerbig, C., Wofsy, S.C., Andrews, A.E., Daube, B.C., Davis, K.J., and Grainger, C.A.:  
777 A near-field tool for simulating the upstream influence of atmospheric observations: The  
778 Stochastic Time-Inverted Lagrangian Transport (STILT) model, *J. Geophys. Res.*, 108(D16), 4493,  
779 doi:10.1029/2002JD003161, 2003.

780 Mao, J., Jacob, D. J., Evans, M. J., Olson, J. R., Ren, X., Brune, W. H., St. Clair, J. M., Crouse,  
781 J. D., Spencer, K. M., Beaver, M. R., Wennberg, P. O., Cubison, M. J., Jimenez, J. L., Fried, A.,  
782 Weibring, P., Walega, P., Hall, S. R., Weinheimer, A. J., Cohen, R. C., Chen, G., Crawford, J. H.,  
783 McNaughton, C., Clarke, A. D., Jaeglé, L., Fisher, J. A., Yantosca, R. M., Le Sager, P., and  
784 Carouge, C.: Chemistry of hydrogen oxide radicals (HO<sub>x</sub>) in the Arctic troposphere in spring,  
785 *Atmos. Chem. Phys.*, 10, 5823–5838, doi:10.5194/acp-10-5823-2010, 2010.

786 Olson, D. M., Dinerstein, E., Wikramanayake, E. D., Burgess, N. D., Powell, G. V. N.,  
787 Underwood, E. C., D'Amico, J. A., I. Itoua, Strand, H.E., Morrison, J. C., Loucks, C. J., Allnutt,  
788 T. F., Ricketts, T. H., Kura, Y., Lamoreux, J. F., Wettengel, W. W., Hedao, P., and Kassem, K.R.:  
789 Terrestrial ecoregions of the world: New map of life on earth, *Bioscience*, 51(11), 933–938, 2001.

790 Olson, J. R., Crawford, J. H., Brune, W., Mao, J., Ren, X., Fried, A., Anderson, B., Apel, E.,  
791 Beaver, M., Blake, D., Chen, G., Crouse, J., Dibb, J., Diskin, G., Hall, S. R., Huey, L. G., Knapp,  
792 D., Richter, D., Riemer, D., St. Clair, J., Ullmann, K., Walega, J., Weibring, P., Weinheimer, A.,  
793 Wennberg, P. O., and Wisthaler, A.: An analysis of fast photochemistry over high northern  
794 latitudes during spring and summer using in-situ observations from ARCTAS and TOPSE, *Atmos.*  
795 *Chem. Phys.*, 12, 6799–6825, doi:10.5194/acp-12-6799-2012, 2012.

796 O'Neill, N. T., Pancrati, O., Baibakov, K., Eloranta, E., Batchelor, R. L., Freemantle, J.,  
797 Lindenmaier, R.: Occurrence of weak, submicron, tropospheric aerosol events at high Arctic  
798 latitudes, *Geophys. Res. Lett.*, 35, L14814, doi:10.1029/2008GL033733, 2008.

799 O'Shea, S. J. , Allen, G., Gallagher, M. W., Bauguitte, S. J.-B., Illingworth, S. M., Le Breton, M.,  
800 Muller, J. B. A., Percival, C. J., Archibald, A. T., Oram, D. E., Parrington, M., Palmer, P. I., and  
801 Lewis, A. C.: Airborne observations of trace gases over boreal Canada during BORTAS: campaign  
802 climatology, air mass analysis and enhancement ratios, *Atmos. Chem. Phys.*, 13, 12451–  
803 12467, doi:10.5194/acp-13-12451-2013, 2013.

804 Oris, F., Asselin, H., Ali, A. A., Finsinger, W., and Bergeron, Y.: Effect of increased fire activity  
805 on global warming in the boreal forest, *Environ. Rev.*, 22, 206–219, doi:10.1139/er-2013-0062,  
806 2013.

807 Palmer, P. I., Parrington, M., Lee, J. D., Lewis, A. C., Rickard, A. R., Bernath, P. F., Duck, T. J.,  
808 Waugh, D. L., Tarasick, D. W., Andrews, S., Aruffo, E., Bailey, L. J., Barrett, E., Bauguitte, S. J.-  
809 B., Curry, K. R., Di Carlo, P., Chisholm, L., Dan, L., Forster, G., Franklin, J. E., Gibson, M. D.,  
810 Griffin, D., Helmig, D., Hopkins, J. R., Hopper, J. T., Jenkin, M. E., Kindred, D., Kliever, J.,  
811 Le Breton, M., Matthiesen, S., Maurice, M., Moller, S., Moore, D. P., Oram, D. E., O'Shea, S. J.,  
812 Owen, R. C., Pagniello, C. M. L. S., Pawson, S., Percival, C. J., Pierce, J. R., Punjabi, S.,  
813 Purvis, R. M., Remedios, J. J., Rotermund, K. M., Sakamoto, K. M., da Silva, A. M.,  
814 Strawbridge, K. B., Strong, K., Taylor, J., Trigwell, R., Tereszchuk, K. A., Walker, K. A.,  
815 Weaver, D., Whaley, C., and Young, J. C.: Quantifying the impact of BOREal forest fires on  
816 Tropospheric oxidants over the Atlantic using Aircraft and Satellites (BORTAS) experiment:  
817 design, execution and science overview, *Atmos. Chem. Phys.*, 13, 6239–6261, doi:10.5194/acp-  
818 13-6239-2013, 2013.

819 Paris, J.-D., Stohl, A., Nédélec, P., Arshinov, M. Y., Panchenko, M. V., Shmargunov, V. P., Law,  
820 K. S., Belan, B. D., and Ciais, P.: Wildfire smoke in the Siberian Arctic in summer: source  
821 characterization and plume evolution from airborne measurements, *Atmos. Chem. Phys.*, 9, 9315–  
822 9327, doi:10.5194/acp-9-9315-2009, 2009.

823 Parrington, M., Palmer, P. I., Lewis, A. C., Lee, J. D., Rickard, A. R., Di Carlo, P., Taylor, J. W.,  
824 Hopkins, J. R., Punjabi, S., Oram, D. E., Forster, G., Aruffo, E., Moller, S. J., Bauguitte, S. J.-B.,  
825 Allan, J. D., Coe, H., and Leigh, R. J.: Ozone photochemistry in boreal biomass burning plumes  
826 *Atmos. Chem. Phys.*, 13, 7321–7341, 2013

827 Paton-Walsh, C., Jones, N. B., Wilson, S. R., Harverd, V., Meier, A., Griffith, D. W. T., and  
828 Rinsland, C. P.: Measurements of trace gas emissions from Australian forest fires and correlations  
829 with coincident measurements of aerosol optical depth, *J. Geophys. Res.*, 110, D24305,  
830 doi:10.1029/2005JD006202, 2005.

831 Paton-Walsh, C., Wilson, S. R., Jones, N. B., and Griffith, D. W. T.: Measurement of methanol  
832 emissions from Australian wildfires by ground-based solar Fourier transform spectroscopy,  
833 *Geophys. Res. Lett.*, 35, L08810, doi:10.1029/2007GL032951, 2008.

834 Paton-Walsh, C., Deutscher, N. M., Griffith, D. W. T., Forgan, B. W., Wilson, S. R., Jones, N. B.,  
835 and Edwards, D. P.: Trace gas emissions from savanna fires in Northern Australia, *J. Geophys.*  
836 *Res.*, 115, D16314, doi:10.1029/2009JD013309, 2010.

837 Paulot, F., Wunch, D., Crouse, J. D., Toon, G. C., Millet, D. B., DeCarlo, P. F., Vigouroux, C.,  
838 Deutscher, N. M., Gonzalez Abad, G., Notholt, J., Warneke, T., Hannigan, J. W., Warneke, C., de  
839 Gouw, J. A., Dunlea, E. J., De Maziere, M., Griffith, D. W. T., Bernath, P., Jimenez, J. L., and  
840 Wennberg, P. O.: Importance of secondary sources in the atmospheric budgets of formic and acetic  
841 acids, *Atmos. Chem. Phys.*, 11, 1989–2013, doi:10.5194/acp-11-1989-2011, 2011.

842 Rinsland, C., Dufour, G., Boone, C., Bernath, P., Chiou, L., Coheur, P., Turquety, S., and  
843 Clerbaux, C.: Satellite boreal measurements over Alaska and Canada during June-July 2004:  
844 Simultaneous measurements of upper tropospheric CO, C<sub>2</sub>H<sub>6</sub>, HCN, CH<sub>3</sub>Cl, CH<sub>4</sub>, C<sub>2</sub>H<sub>2</sub>, CH<sub>3</sub>OH,  
845 HCOOH, OCS, and SF<sub>6</sub> mixing ratios, *Global Biogeochem. Cy.*, 21, GB3008,  
846 doi:10.1029/2006GB002795, 2007.

847 Rodgers, C. D.: Inverse methods for atmospheric sounding theory and practise, in: Series on  
848 Atmospheric, Oceanic and Planetary Physics, Vol. 2, World Scientific, London, 238 pp., 2000.

849 Rodgers, C. D., and Connor, B. J.: Intercomparison of remote sounding instruments, *J. Geophys.*  
850 *Res.*, 108(D3), 4116–4129, doi:10.1029/2002JD002299, 2003.

851 Rothman, L. S., Gordon, I. E., Barbe, A., Benner, D. C., Bernath, P. F., Birk, M., Boudon, V.,  
852 Brown, L. R., Campargue, A., Champion, J.-P., Chance, K., Coudert, L. H., Danaj, V., Devi, V.  
853 M., Fally, S., Flaud, J.-M., Gamache, R. R., Goldman, A., Jacquemart, D., Kleiner, I., Lacombe,  
854 N., Lafferty, W. J., Mandin, J.-Y., Massie, S. T., Mikhailenko, S. N., Miller, C. E., Moazzen-  
855 Ahmadi, N., Naumenko, O. V., Nikitin, A. V., Orphal, J., Perevalov, V. I., Perrin, A., Predoi-  
856 Cross, A., Rinsland, C. P., Rotger, M., Simeckova, M., Smith, M. A. H., Sung, K., Tashkun, S. A.,  
857 Tennyson, J., Toth, R. A., Vandaele, A. C., and Vander Auwera, J.: The Hitran 2008 molecular  
858 spectroscopic database, *J. Quant. Spectrosc. Radiat. Transfer*, 110, 533–572,  
859 doi:10.1016/j.jqsrt.2009.02.013, 2009.

860 Saha, A., O'Neill, N. T., Eloranta, E., Stone, R. S., Eck, T. F., Zidane, S., McArthur, L. J. B.: Pan-  
861 Arctic sunphotometry during the ARCTAS-A campaign of April 2008, *Geophys. Res. Lett.*, 37,  
862 L05803, doi:10.1029/2009GL041375, 2010.

863 Oris, F., Asselin, H., Ali, A. A., Finsinger, W., Bergeron, Y.: Effect of increased fire activity on  
864 global warming in the boreal forest, *Environmental Reviews*, , 1–14, doi:10.1139/er-2013-0062,  
865 2013.

866 Shindell, D. T., Chin, M., Dentener, F., Doherty, R. M., Faluvegi, G., Fiore, A. M., Hess, P., Koch,  
867 D. M., MacKenzie, I. A., Sanderson, M. G., Schultz, M. G., Schulz, M., Stevenson, D. S., Teich,  
868 H., Textor, C., Wild, O., Bergmann, D. J., Bey, I., Bian, H., Cuvelier, C., Duncan, B. N., Folberth,  
869 G., Horowitz, L. W., Jonson, J., Kaminski, J. W., Marmer, E., Park, R., Pringle, K. J., Schroeder,  
870 S., Szopa, S., Takemura, T., Zeng, G., Keating, T. J., and Zuber, A.: A multi-model assessment of  
871 pollution transport to the Arctic, *Atmos. Chem. Phys.*, 8, 5353–5372, doi:10.5194/acp-8-5353-  
872 2008, 2008.

873 Simpson, I. J., Akagi, S. K., Barletta, B., Blake, N. J., Choi, Y., Diskin, G. S., Fried, A., Fuelberg,  
874 H. E., Meinardi, S., Rowland, F. S., Vay, S. A., Weinheimer, A. J. P., Wennberg, P. O., Wiebring,  
875 P., Wisthaler, A., Yang, M., Yokelson, R. J., and Blake, D. R.: Boreal forest fire emissions in fresh  
876 Canadian smoke plumes: C<sub>1</sub>-C<sub>10</sub> volatile organic compounds (VOCs), CO<sub>2</sub>, CO, NO<sub>2</sub>, NO, HCN  
877 and CH<sub>3</sub>CN, *Atmos. Chem. Phys.*, 11, 6445–6463, doi:10.5194/acp-11-6445–2011, 2011.

878 Soja, A.J., Tchepakova, N.M., French, N.H.F., Flannigan, M.D., Shugart, H.H., Stocks, B.J.,  
879 Sukhinin, A.I., Parfenova, E.I., Chapin, F.S., and Stackhouse, P.W.: Climate - induced boreal  
880 forest change: Predictions versus current observations, *Global and Planetary Change*, 56, 274–296,  
881 doi:10.1016/j.gloplacha.2006.07.028, 2007.

882 Stavrakou, T., Müller, J.-F., De Smedt, I., Van Roozendael, M., van der Werf, G. R., Giglio, L.,  
883 and Guenther, A.: Evaluating the performance of pyrogenic and biogenic emission inventories  
884 against one decade of space-based formaldehyde columns, *Atmos. Chem. Phys.*, 9, 1037–1060,  
885 doi:10.5194/acp-9-1037-2009, 2009.

886 Stavrakou, T., Müller, J.-F., Peeters, J., Razavi, A., Clarisse, L., Clerbaux, C., Coheur, P.-F.,  
887 Hurtmans, D., De Mazière, M., Vigouroux, C., Deutscher, N. M., Griffith, D. W. T., Jones, N. and  
888 Paton-Walsh, C.: Satellite evidence for a large source of formic acid from boreal and tropical  
889 forests, *Nature Geoscience*, 5, 26–30, doi:10.1038/ngeo1354, 2012.

890 Stohl, A.: Characteristics of atmospheric transport into the Arctic troposphere, *J. Geophys. Res.*,  
891 111, D11306, doi:10.1029/2005JD006888, 2006.

892 Stohl, A., Berg, T., Burkhart, J. F., Fjæraa, A. M., Forster, C., Herber, A., Hov, Ø., Lunder, C.,  
893 McMillan, W. W., Oltmans, S., Shiobara, M., Simpson, D., Solberg, S., Stebel, K., Strom,  
894 J., Tørseth, K., Treffeisen, R., Virkkunen, K., and Yttri, K. E.: Arctic smoke - record air pollution  
895 levels in the European Arctic during a period of abnormal warmth, due to agricultural fires in  
896 Eastern Europe, *Atmos. Chem. Phys.*, 7, 511–534, doi:10.5194/acp-7-511-2007, 2007.

897 Tereszchuk, K. A., Gonzalez Abad, G., Clerbaux, C., Hurtmans, D., Coheur, P.-F., and Bernath,  
898 P. F.: ACE-FTS measurements of trace species in the characterization of biomass burning plumes,  
899 *Atmos. Chem. Phys.*, 11, 12169–12179, doi:10.5194/acp-11-12169-2011, 2011.

900 Tereszchuk, K. A., González Abad, G., Clerbaux, C., Hadji-Lazaro, J., Hurtmans, D., Coheur, P.-  
901 F., and Bernath, P. F.: ACE-FTS observations of pyrogenic trace species in boreal biomass burning  
902 plumes during BORTAS, *Atmos. Chem. Phys.*, 13, 4529–4541, doi:10.5194/acp-13-4529-2013,  
903 2013.

904 Thomas, J. L., Raut, J.-C., Law, K. S., Marelle, L., Ancellet, G., Ravetta, F., Fast, J. D., Pfister,  
905 G., Emmons, L. K., Diskin, G. S., Weinheimer, A., Roiger, A., and Schlager, H.: Pollution  
906 transport from North America to Greenland during summer 2008, *Atmos. Chem. Phys.*, 13, 3825–  
907 3848, doi:10.5194/acp-13-3825-2013, 2013.

908 Tilmes, S., Emmons, L. K., Law, K. S., Ancellet, G., Schlager, H., Paris, J.-D., Fuelberg, H. E.,  
909 Streets, D. G., Wiedinmyer, C., Diskin, G. S., Kondo, Y., Holloway, J., Schwarz, J. P., Spackman,  
910 J. R., Campos, T., Ndlele, P., and Panchenko, M. V.: Source contributions to Northern Hemisphere  
911 CO and black carbon during spring and summer 2008 from POLARCAT and  
912 START08/preHIPPO observations and MOZART-4, *Atmos. Chem. Phys. Discuss.*, 11, 5935–  
913 5983, doi:10.5194/acpd-11-5935-2011, 2011.

914 Viatte, C., Strong, K., Paton-Walsh, C., Mendonca, J., O'Neill, N. T., and Drummond, J. R.:  
915 Measurements of CO, HCN and C<sub>2</sub>H<sub>6</sub> total columns in smoke plumes transported from the 2010  
916 Russian boreal forest fires to the Canadian high Arctic, *Atmosphere-Ocean*, 51, 1–10,  
917 doi:10.1080/07055900.2013.823373, 2013.

918 Viatte, C., Strong, K., Walker, K. A., and Drummond, J. R.: Five years of CO, HCN, C<sub>2</sub>H<sub>6</sub>, C<sub>2</sub>H<sub>2</sub>,  
919 CH<sub>3</sub>OH, HCOOH, and H<sub>2</sub>CO total columns measured in the Canadian High Arctic, *Atmos. Meas.*  
920 *Tech.*, 7, 1547–1570, doi:10.5194/amt-7-1547-2014, 2014.

921 Vigouroux, C., Stavrakou, T., Whaley, C., Dils, B., Duflot, V., Hermans, C., Kumps, N., Metzger,  
922 J.-M., Scolas, F., Vanhaelewyn, G., Müller, J.-F., Jones, D. B. A., Li, Q., and De Mazière, M.:  
923 FTIR time-series of biomass burning products (HCN, C<sub>2</sub>H<sub>6</sub>, C<sub>2</sub>H<sub>2</sub>, CH<sub>3</sub>OH, and HCOOH) at  
924 Reunion Island (21°S, 55°E) and comparisons with model data, *Atmos. Chem. Phys.*, 12, 10367–  
925 10385, doi:10.5194/acp-12-10367-2012, 2012.

926 Warneke, C., Bahreini, R., Brioude, J., Brock, C.A., de Gouw, J.A., Fahey, D.W., Froyd, K.D.,  
927 Holloway, J.S., Middlebrook, A., Miller, L., Montzka, S., Murphy, D.M., Peischl, J., Ryerson,  
928 T.B., Schwarz, J.P., Spackman, J.R., and Veres, P.: Biomass burning in Siberia and Kazakhstan as  
929 an important source for haze over the Alaskan Arctic in April 2008, *Geophys. Res. Lett.*, 36,  
930 L02813, doi:10.1029/2008GL036194, 2009.

931 Wang, Q., Jacob, D. J., Fisher, J. A., Mao, J., Leibensperger, E. M., Carouge, C. C., Le Sager, P.,  
932 Kondo, Y., Jimenez, J. L., Cubison, M. J., and Doherty, S. J.: Sources of carbonaceous aerosols  
933 and deposited black carbon in the Arctic in winter-spring: implications for radiative forcing,  
934 *Atmos. Chem. Phys.*, 11, 12453–12473, doi:10.5194/acp-11-12453-2011, 2011.

935 Wiedinmyer, C., Akagi, S. K., Yokelson, R. J., Emmons, L. K., Al-Saadi, J. A., Orlando, J. J., and  
936 Soja, A. J.: The Fire INventory from NCAR (FINN): a high resolution global model to estimate  
937 the emissions from open burning, *Geosci. Model Dev.*, 4, 625–641, doi:10.5194/gmd-4-625-2011,  
938 2011.

939 Xiao, Y., Jacob, D. J., and Turquety, S.: Atmospheric acetylene and its relationship with CO as an  
940 indicator of air mass age, *J. Geophys. Res.*, 112, D12305, doi:10.1029/2006JD008268, 2007.

941 Xiao, Y., Logan, J. A., Jacob, D. J., Hudman, R. C., Yantosca, R., and Blake, D. R.: Global budget  
942 of ethane and regional constraints on US sources, *J. Geophys. Res.*, 113, D21306,  
943 doi:10.1029/2007JD009415, 2008.

944 Yokelson, R. J., Andreae, M. O., and Akagi, S. K.: Pitfalls with the use of enhancement ratios or  
945 normalized excess mixing ratios measured in plumes to characterize pollution sources and aging,  
946 *Atmos. Meas. Tech.*, 6, 2155-2158, doi:10.5194/amt-6-2155-2013, 2013.

947 York, D., Evensen, N. M., Lopez Martinez, M., and De Basabe Delgado, J.: Unified equations for  
948 the slope, intercept, and standard errors of the best straight line, *Am J. Phys.*, 72(3), 367–375,  
949 <http://dx.doi.org/10.1119/1.1632486>, 2004.

950 Young, E., and Paton-Walsh, C.: Emission Ratios of the Tropospheric Ozone Precursors Nitrogen  
951 Dioxide and Formaldehyde from Australia's Black Saturday Fires, *Atmosphere*, 2, 617-632,  
952 doi:10.3390/atmos2040617, 2011.

953 Yurganov, L. N., Blumenstock, T., Grechko, E. I., Hase, F., Hyer, E. J., Kasischke, E. S., Koike,  
954 M., Kondo, Y., Kramer, I., Leung, F.-Y., Mahieu, E., Mellqvist, J., Notholt, J., Novelli, P. C.,  
955 Rinsland, C. P., Scheel, H. E., Schulz, A., Strandberg, A., Sussmann, R., Tanimoto, H., Velazco,  
956 V., Zander, R. and Zhao, Y.: A quantitative assessment of the 1998 carbon monoxide emission  
957 anomaly in the Northern Hemisphere based on total column and surface concentration  
958 measurements, *J. Geophys. Res.*, 109, D15305, doi:10.1029/2004JD004559, 2004.

959 Yurganov, L. N., Duchatelet, P., Dzhola, A. V., Edwards, D. P., Hase, F., Kramer, I., Mahieu, E.,  
960 Mellqvist, J., Notholt, J., Novelli, P. C., Rockmann, A., Scheel, H. E., Schneider, M., Schulz, A.,  
961 Strandberg, A., Sussmann, R., Tanimoto, H., Velazco, V., Drummond, J. R., and Gille, J. C.:  
962 Increased Northern Hemispheric carbon monoxide burden in the troposphere in 2002 and 2003  
963 detected from the ground and from space, *Atmos. Chem. Phys.*, 5, 563–573, 2005.

964 Zeng, G., Wood, S. W., Morgenstern, O., Jones, N. B., Robinson, J., and Smale, D.: Trends and  
965 variations in CO, C<sub>2</sub>H<sub>6</sub>, and HCN in the Southern Hemisphere point to the declining anthropogenic  
966 emissions of CO and C<sub>2</sub>H<sub>6</sub>, *Atmos. Chem. Phys.*, 12, 7543–7555, doi:10.5194/acp-12-7543-2012,  
967 2012.

968

969

year	month	days of measurement	fire source		travel time used to calculate ER
			vegetation type	location	
2008	March	20, 21, 23, 24, <b>25</b> , 27, 28, 29, 30, 31	boreal	Russia	7 days
2008	April	<b>12</b> , 14, 15, 16, 17, 19	temperate coniferous and grassland	Central USA	5 days
2008	July	<b>10</b> , 12, 21, 22, 23, 29	boreal	Russia	5 days
2009	June	2, 3, <b>5</b> , 6, 8, 9, 10	boreal	Russia	6 days
2010	May	<b>14</b> , 16, 17, 21, 22	temperate coniferous and grassland	Central USA	7 days
2010	July	3, <b>5</b> , 6, 9	boreal	Central Canada and Alaska	6 days
2010	August	9, 10, <b>12</b> , 13, 14, 16, 18, 19, 20, 22, <b>23</b> , 24, 25, 28, 29	boreal	Fire in Russia in Moscow Area	9 days
2011	June	6, 7, 8, <b>9</b> , 10, 11, 13	boreal and temperate coniferous and grassland	Central USA, Canada	8 days
2011	June/July	27, <b>28</b> , 29, 30, 1, 2, 4, 5	boreal	Canada	6 days
2012	July	<b>1</b> , 2, 3, 4	boreal and temperate coniferous and grassland	Canada, Central USA	5 days

971

972 Table 1: Fire events detected over Eureka with the date, days of measurements, vegetation type  
973 burned, fire source location, and travel time to the day of peak enhancement (represented bold in  
974 the third column) used to calculate emission ratios.

year	month	days of measurement	fire source		travel time used to calculate ER
			vegetation type	location	
2008	March	<b>24</b> , 25, 26, 27, 29, 30, 31	boreal	Russia	7 days
2008	August	2, <b>4</b> , 5, 6, 7, 9	boreal	Central Canada	5 days
2010	July	<b>30</b> , 31, 3	boreal	Canada	5 days
2010	August	23, <b>24</b> , 25, 26, 27, 28, 29, 2	boreal	Fire in Russia in Moscow Area	9 days
2011	June	21, 22, 25, 26, 27, <b>28</b> , 29	boreal	Canada	6 days
2011	July	20, 21, 23, <b>24</b> , 26, 27	boreal	Canada	6 days
2012	April/May	27, 28, 29, <b>8</b> , 9, 10, 11, 12, 13, 14	boreal and temperate coniferous and grassland	Russia	7 days
2012	July	<b>15</b> , 16, 18, 19, 20, 22, 29, 30, 31, 1	boreal	Canada, Central USA	5 days

976 Table 2: Same as Table 1 but for Thule.

gas	columns	N	r	relative difference (%) (model-FTIR)/model	SD (%)	slope (MOZART-4 vs. FTIR)	error on slope	error bar on FTIR total column (%)	lifetime of gas (days)
CO	tropo	1001	0.879	2.888	7.532	0.667	0.011	3.1	30
HCN	tropo	423	0.921	-6.714	19.320	0.468	0.010	10.5	30-180
C <sub>2</sub> H <sub>6</sub>	tropo	452	0.849	50.282	22.680	0.506	0.015	14.3	45
C <sub>2</sub> H <sub>2</sub>	tot	289	0.927	137.047	329.439	1.548	0.037	22.5	15
CH <sub>3</sub> OH	tot	315	0.769	23.296	23.434	0.586	0.028	12.3	5-10
HCOOH	tot	270	0.605	1504.406	894.834	0.049	0.004	17	3-4
H <sub>2</sub> CO	tot	445	0.494	82.057	141.583	0.357	0.030	27.5	<2

978

979 Table 3: Results of the 2008-2012 comparisons between MOZART-4 and the FTIR columns  
980 measured at Eureka for the seven species listed in the first column. The comparisons are made for  
981 the tropospheric columns (0.6-10.25 km) for CO, HCN and C<sub>2</sub>H<sub>6</sub> and for the total columns (for  
982 the other gases). N is the number of points included in the comparisons and r is the coefficient of  
983 linear correlation. The relative differences (in percentage) are calculated as (model-FTIR)/model,  
984 SD is the one-sigma standard deviation around the mean difference. **The last four** columns are the  
985 slopes of the linear regression lines between MOZART-4 and FTIR along with their errors, the  
986 error bars on the FTIR total columns (in percentage), **and the atmospheric lifetimes of the target**  
987 **species.**

988

gas	columns	N	r	relative difference (%)(model- FTIR)/model	SD (%)	slope (MOZART-4 vs. FTIR)	error on slope
CO	tropo	145	0.736	-2.48	11.37	0.529	0.041
HCN	tropo	111	0.555	2.24	19.45	0.222	0.027
C <sub>2</sub> H <sub>6</sub>	tropo	277	0.829	-54.14	29.73	0.431	0.018
C <sub>2</sub> H <sub>2</sub>	tot	139	0.908	-102.14	159.10	1.145	0.045
CH <sub>3</sub> OH	tot	118	0.620	1.93	40.79	0.390	0.046
HCOOH	tot	138	0.349	-1538.70	831.12	0.010	0.002
H <sub>2</sub> CO	tot	137	0.753	-152.81	129.67	0.426	0.032

989

990 Table 4: Same as Table 3 but for Thule.

991

gas	Year	2008	2008	2008	2009	2010	2010	2010	2011	2011	2012	mean ± SD
	Month	March	April	July	June	May	July	August	June	June/July	July	
HCN	N	20	20	16	48	32	12	66	44	38	17	
	r	0.85	0.94	0.97	0.76	0.7	0.88	0.82	0.85	0.92	0.67	0.84 ± 0.10
	EnhRx10 <sup>-3</sup>	2.4	3.83	3.6	3.37	3.26	4.01	6.2	3.19	2.55	2.75	3.52 ± 1.08
	ER	2.23	3.64	3.42	3.17	3.03	3.77	5.63	2.93	2.40	3.25	3.34 ± 0.94
C <sub>2</sub> H <sub>6</sub>	N	30	22	16	49	32	12	64	41	38	17	
	r	0.62	0.87	0.97	0.68	0.9	0.72	0.9	0.68	0.86	0.86	0.81 ± 0.12
	EnhRx10 <sup>-3</sup>	5.15	10.30	7.34	14.25	10.65	4.27	9.69	13.04	9.98	5.23	8.99 ± 3.40
	ER	5.36	10.60	7.55	14.74	11.08	4.42	10.19	13.63	10.32	7.77	9.56 ± 3.19
C <sub>2</sub> H <sub>2</sub>	N	20	21	13	48	31		30	14	20	8	
	r	0.76	0.93	0.92	0.87	0.78		0.63	0.61	0.93	0.55	0.78 ± 0.15
	EnhRx10 <sup>-3</sup>	2.36	4.16	2.24	5.71	2.93		1.36	3.80	2.45	0.98	2.89 ± 1.47
	ER	3.11	5.16	2.78	7.32	3.87		1.89	5.15	3.14		4.05 ± 1.74
CH <sub>3</sub> OH	N		6	16	48	11	10	45	18	39	35	
	r		0.76	0.86	0.3	0.12	0.86	0.9	0.74	0.88	0.42	0.64 ± 0.29
	EnhRx10 <sup>-3</sup>		10.69	10.70	42.45	500.79*	24.57	16.89	70.22	28.23	19.62	25.85 ± 20.63
	ER		15.70	15.71			37.64	28.37	114.91*	43.24		28.13 ± 12.52
HCOOH	N	28	21	10	44	27	6	38	9	19		
	r	0.87	0.75	0.93	0.74	0.53	0.97	0.67	0.78	0.83		0.79 ± 0.13
	EnhRx10 <sup>-3</sup>	6.30	10.42	2.69	7.48	8.34	8.10	3.14	22.14	4.13		8.08 ± 5.87
	ER	11.37	17.60	11.13	13.12		14.21	5.90	40.86	8.30		15.31 ± 4.03
H <sub>2</sub> CO	N	16	18	16	38	28	12	64	43	45	18	
	r	0.08	0.58	0.64	0.15	-0.09	0.51	0.16	0.42	0.74	0.9	0.41 ± 0.32
	EnhRx10 <sup>-3</sup>	159.2*	4.13	1.38	8.16	7.17	2.92	3.41	12.13	4.28	7.4	5.37 ± 3.86

992

993 Table 5: Correlation between each trace gas and CO inside the smoke plumes detected over Eureka.

994 N is the number of points, r is the coefficient of linear correlation and 'EnhR' is the enhancement

995 ratio, which is the slope derived from the correlation. For all gases except H<sub>2</sub>CO, ER represents

996 the corrected enhancement ratios from travel time (calculated only if the linear correlation

997 coefficient (r > 0.6) and the number of points (N >= 6)). \*Values excluded from the mean

998 calculations.

999

1000

gas	Year Month	2008 March	2008 August	2010 July	2010 August	2011 June	2011 July	2012 April/May	2012 July	mean ± SD
HCN	N	17	20	9	34	12	17	9	18	
	r	0.42	0.79	0.96	0.79	0.8	0.87	0.8	0.85	0.79 ± 0.16
	EnhRx10 <sup>-3</sup>	4.20	6.09	8.24	7.16	1.60	3.06	1.93	2.95	4.40 ± 2.48
	ER		5.78	7.83	6.50	1.50	2.87	1.79	3.75	4.29 ± 2.45
C <sub>2</sub> H <sub>6</sub>	N	33	44	16	64	23	35	25	34	
	r	0.85	0.14	0.93	0.89	0.92	0.89	0.95	0.9	0.81 ± 0.27
	EnhRx10 <sup>-3</sup>	17.27	-0.02	17.98	11.75	10.10	6.33	11.56	6.73	10.21 ± 5.93
	ER	17.96		18.50	12.35	10.45	6.55	12.02	6.92	12.11 ± 4.76
C <sub>2</sub> H <sub>2</sub>	N	17	21	9	34	12	17	9	18	
	r	0.58	0.63	0.85	0.76	0.88	0.91	0.88	0.91	0.80 ± 0.13
	EnhRx10 <sup>-3</sup>	2.58	1.88	3.56	1.37	1.88	2.22	2.52	1.92	2.24 ± 0.66
	ER		2.33	4.42	1.91	2.41	2.84	3.33	2.38	2.80 ± 0.84
CH <sub>3</sub> OH	N									
	r									
	EnhRx10 <sup>-3</sup>									
HCOOH	N	13	19	8	30	9	14	11	16	
	r	0.55	0.87	-0.71	0.76	0.84	0.65	0.88	0.77	0.58 ± 0.53
	EnhRx10 <sup>-3</sup>	3.80	13.78	-4.47	10.77	12.12	1.57	15.93	6.58	7.51 ± 6.92
	ER		23.27		20.22	21.26	2.75	28.76	11.11	17.90 ± 9.37
H <sub>2</sub> CO	N	30	23	6	30	11	18	15	16	
	r	0.64	0.34	-0.55	0.57	0.93	0.38	0.56	0.3	0.40 ± 0.43
	EnhRx10 <sup>-3</sup>	6.02	3.85	-1.76	3.70	11.79	2.21	3.58	2.52	3.99 ± 3.85

1001

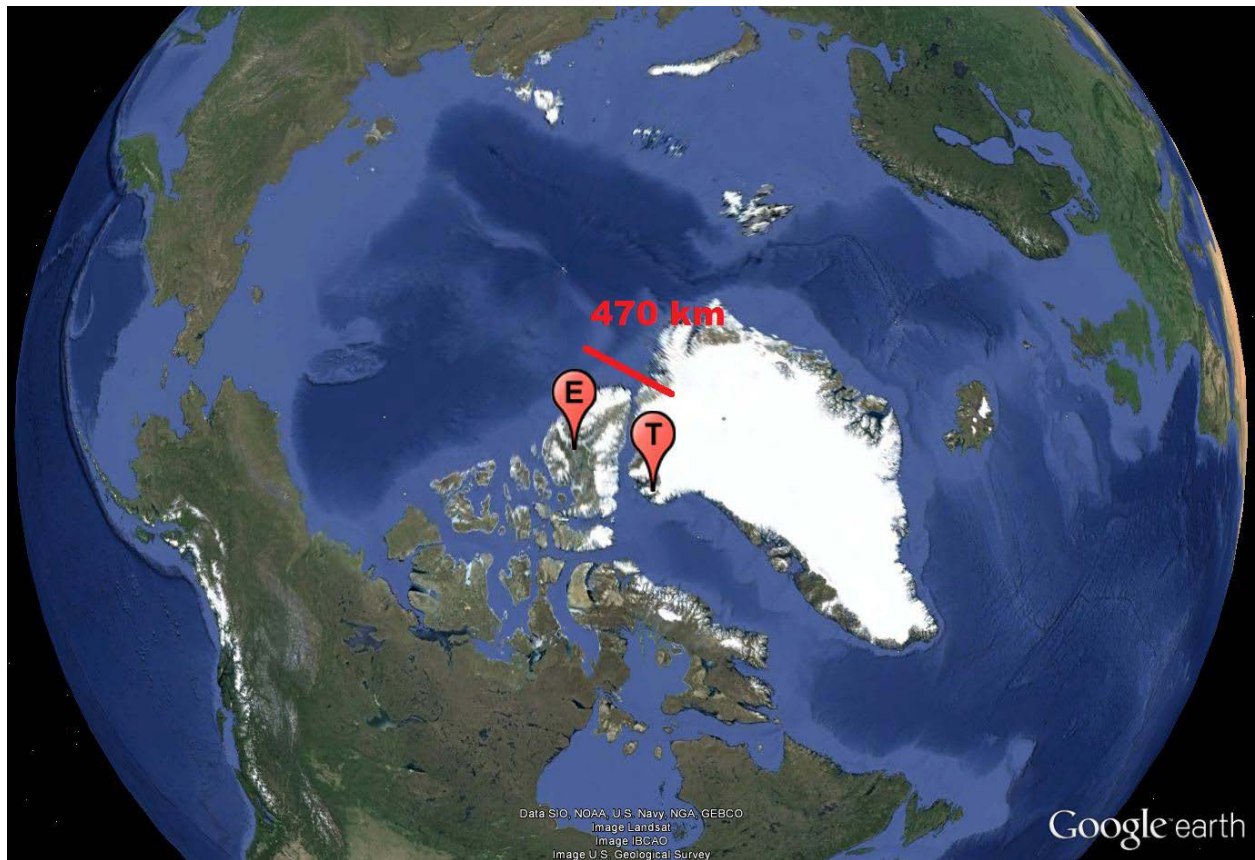
1002 Table 6: Correlation between each trace gas and CO inside the smoke plumes detected over Thule.  
1003 N is the number of points, r is the coefficient of linear correlation and 'EnhR' are the Enhancement  
1004 Ratios, which are the slopes derived from the correlation. For all gases except H<sub>2</sub>CO, ER represents  
1005 the corrected enhancement ratios from travel time (calculated only if the linear correlation  
1006 coefficient (r > 0.6) and the number of points (N >= 6)). \*Values excluded from the mean  
1007 calculations.

1008

	Eureka		Thule	
	mean ER $\pm$ SD	mean EF $\pm$ SD	mean ER $\pm$ SD	mean EF $\pm$ SD
HCN	0.00334 $\pm$ 0.00094	0.36 $\pm$ 0.17	0.00429 $\pm$ 0.00245	0.44 $\pm$ 0.25
C <sub>2</sub> H <sub>6</sub>	0.00956 $\pm$ 0.00319	1.09 $\pm$ 0.74	0.01211 $\pm$ 0.00476	1.39 $\pm$ 0.68
C <sub>2</sub> H <sub>2</sub>	0.00405 $\pm$ 0.00174	0.40 $\pm$ 0.25	0.00280 $\pm$ 0.00084	0.28 $\pm$ 0.18
CH <sub>3</sub> OH	0.02813 $\pm$ 0.01252	3.44 $\pm$ 1.68		
HCOOH	0.01531 $\pm$ 0.00403	2.69 $\pm$ 1.14	0.01790 $\pm$ 0.00937	3.15 $\pm$ 1.46

1009

1010 Table 7: Means and one-sigma standard deviations of equivalent emission ratios and emission  
1011 factors (using EF<sub>co</sub> for the extratropical forest) calculated from FTIR measurements performed at  
1012 Eureka and Thule for HCN, C<sub>2</sub>H<sub>6</sub>, C<sub>2</sub>H<sub>2</sub>, CH<sub>3</sub>OH, and HCOOH. Standard deviations are smaller  
1013 than in Tables 5 and 6 because filters (using threshold values on the linear correlation coefficient  
1014 ( $r > 0.6$ ) and the number of points ( $N \geq 6$ )) were applied in the calculation of equivalent emission  
1015 ratios.

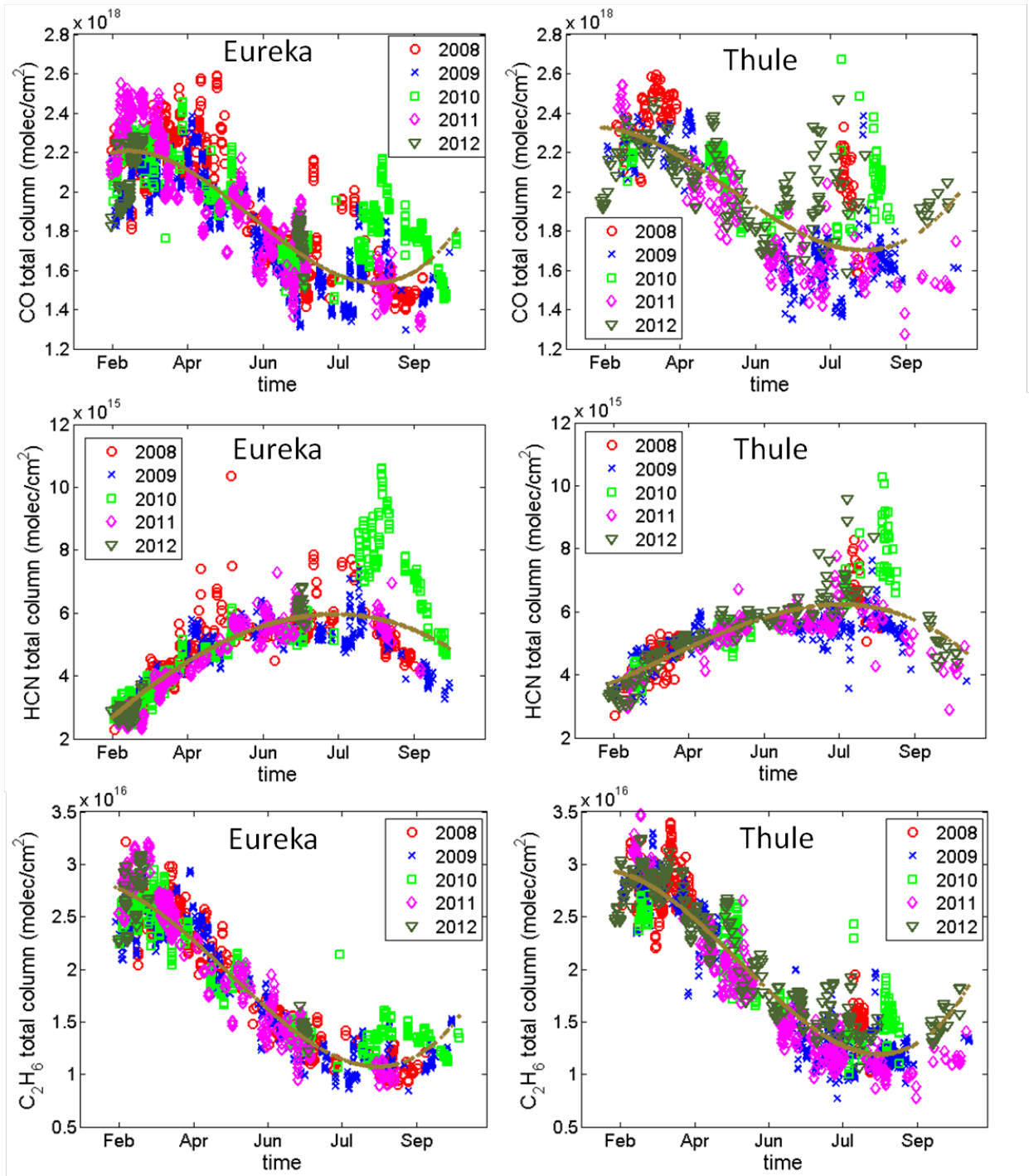


1016

1017 Figure 1: Locations of the FTIR measurements at Eureka (E) and Thule (T) (map provided by  
1018 GOOGLE EARTH V 7.0.3.8542, US Dept. of State Geographer, Google, 2012, Image Landsat,  
1019 Data SIO, NOAA, U.S, Navy, NGA, and GEBCO).

1020

1021

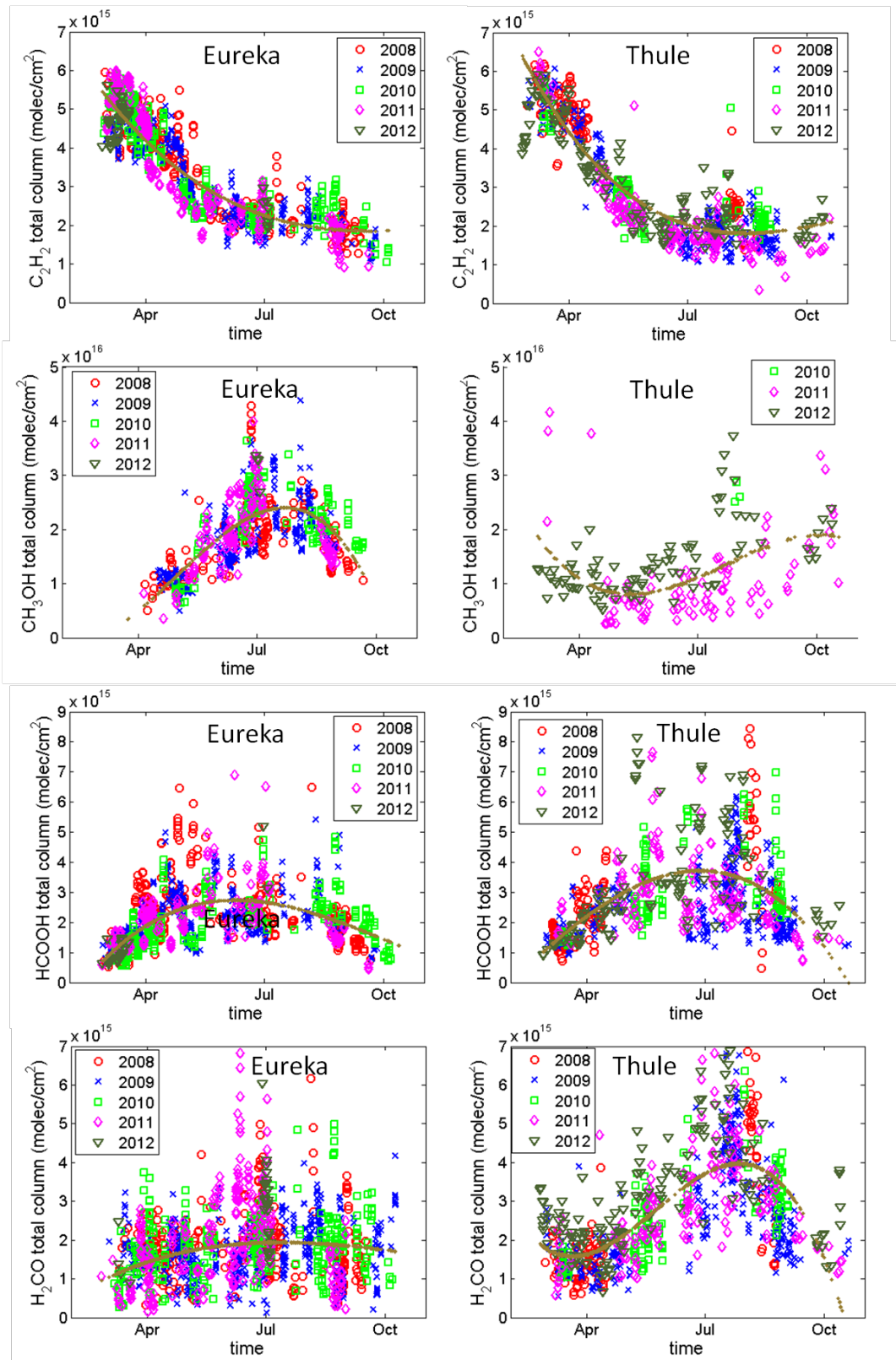


1022

1023 Figure 2: Timeseries of CO, HCN, and C<sub>2</sub>H<sub>6</sub> total columns measured at Eureka (left panels) and  
 1024 Thule (right panels) from 2008 to 2012. The brown lines represent the polynomial fits to the data.

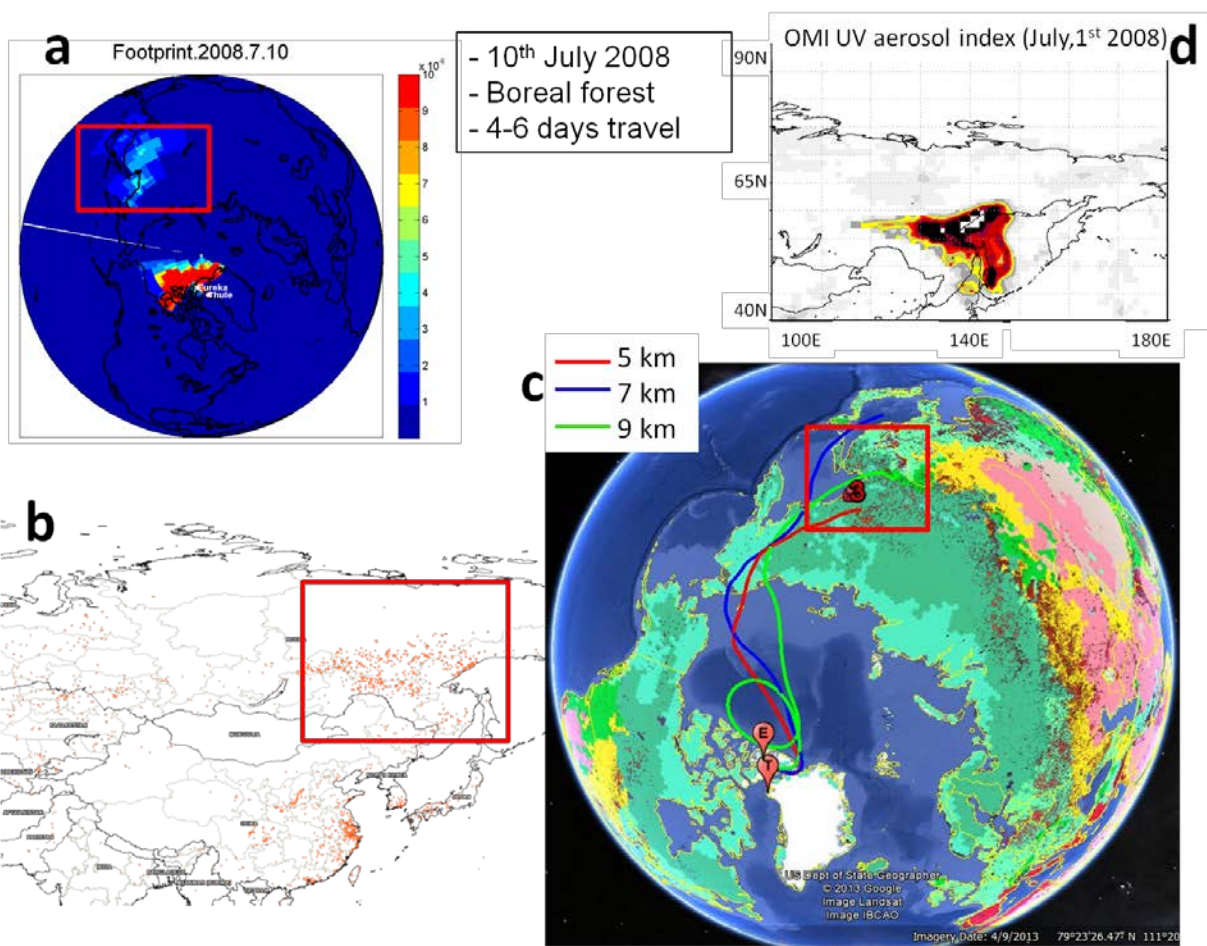
1025

1026



1027

1028 Figure 3: Timeseries of  $C_2H_2$ ,  $CH_3OH$ ,  $HCOOH$  and  $H_2CO$  total columns measured at Eureka (left  
 1029 panels) and Thule (right panels) from 2008 to 2012. The brown lines represent the polynomial fits  
 1030 to the data.

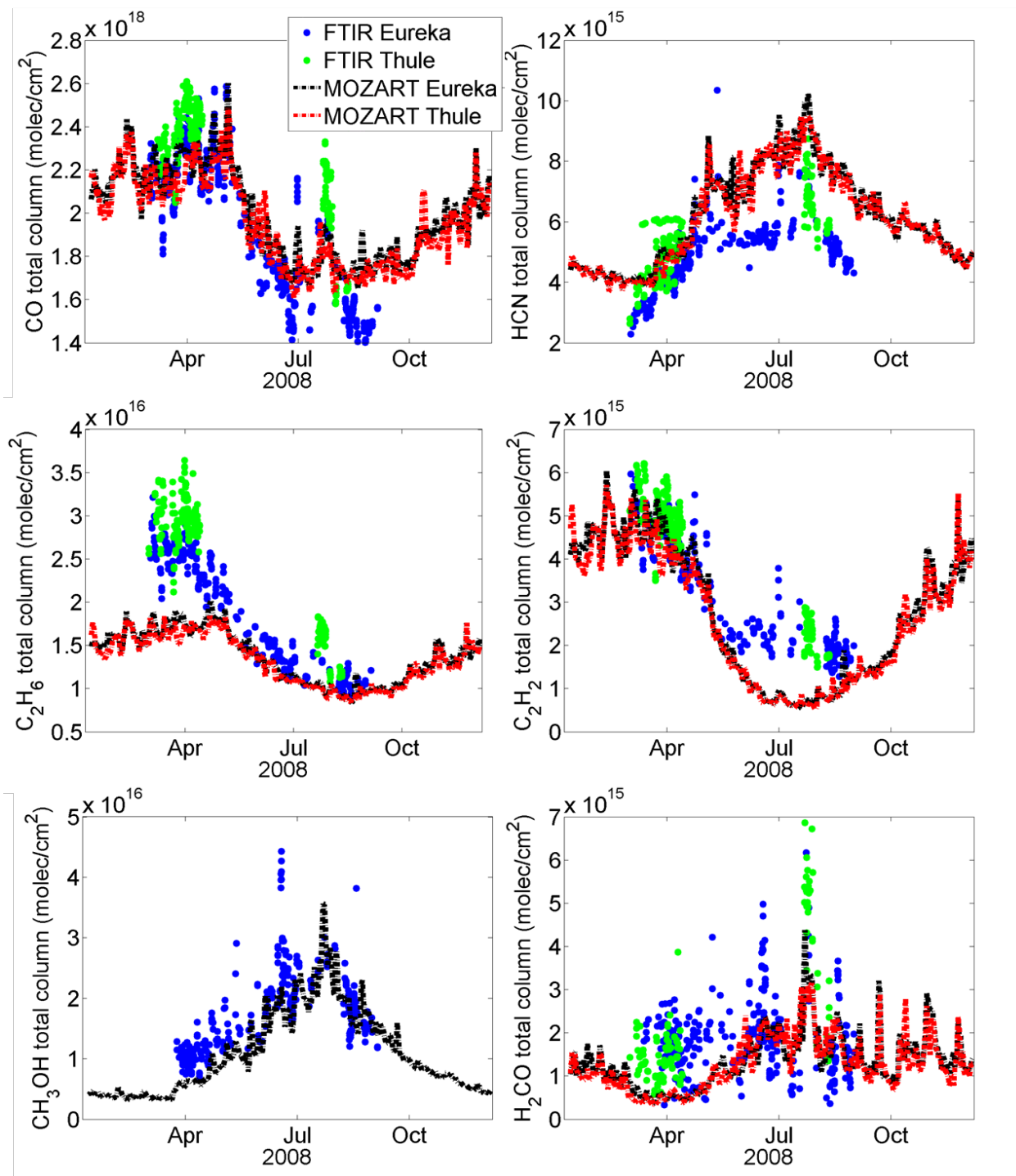


1031

1032 Figure 4: Example of attribution of fire source region and transport time for the event number 3,  
 1033 detected at Eureka on the 10<sup>th</sup> of July, 2008. a) STILT footprints for that day, b) MODIS fire hot  
 1034 spots, c) HYSPLIT backtrajectories ending that day, d) OMI UV aerosol index for that day.

1035

1036

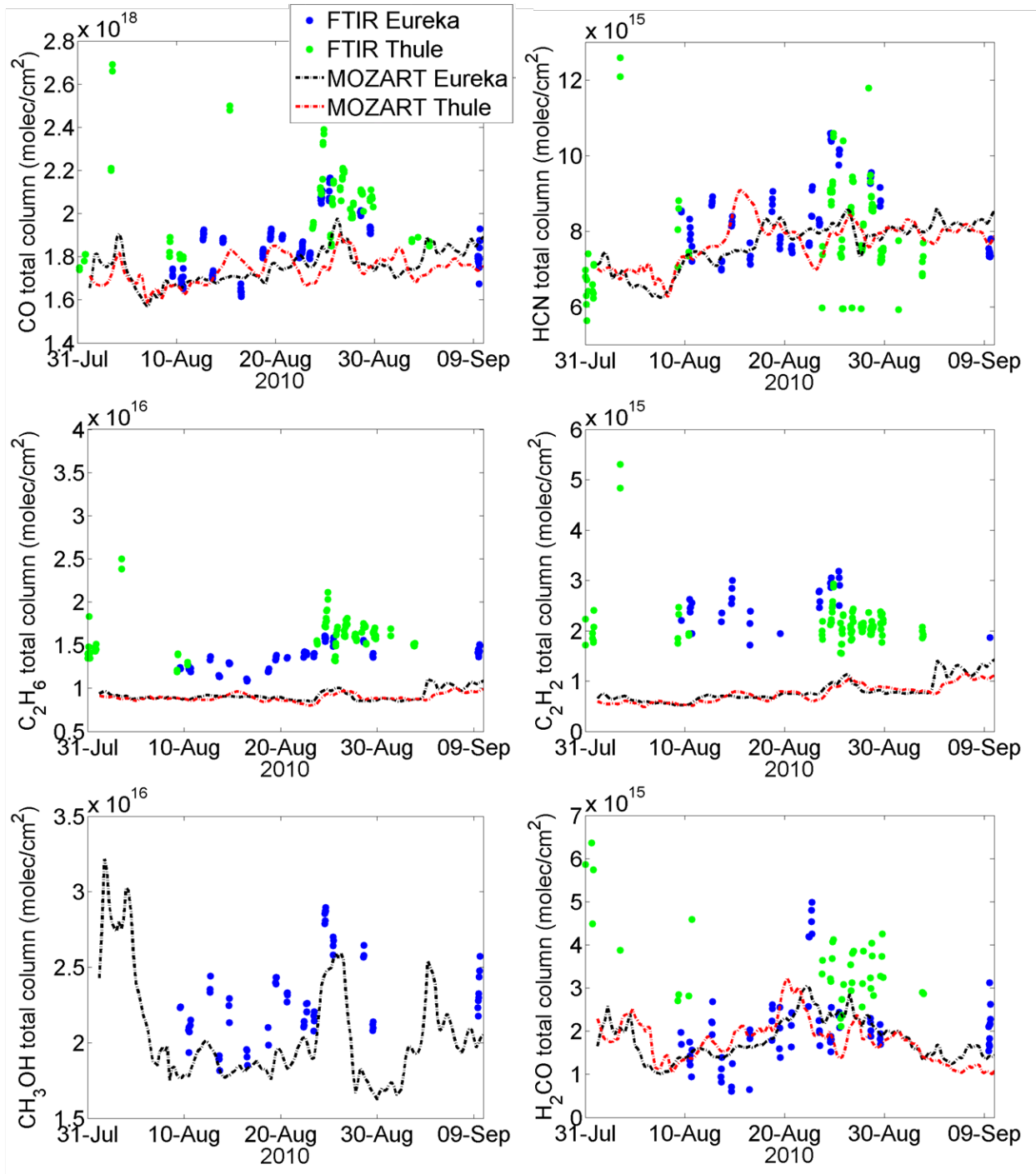


1037

1038 Figure 5: Timeseries of CO, HCN, C<sub>2</sub>H<sub>6</sub>, C<sub>2</sub>H<sub>2</sub>, CH<sub>3</sub>OH, and H<sub>2</sub>CO total columns measured by the  
 1039 FTIRs at Eureka (blue) and Thule (green) and calculated by MOZART-4 at Eureka (black) and  
 1040 Thule (red) for 2008.

1041

1042

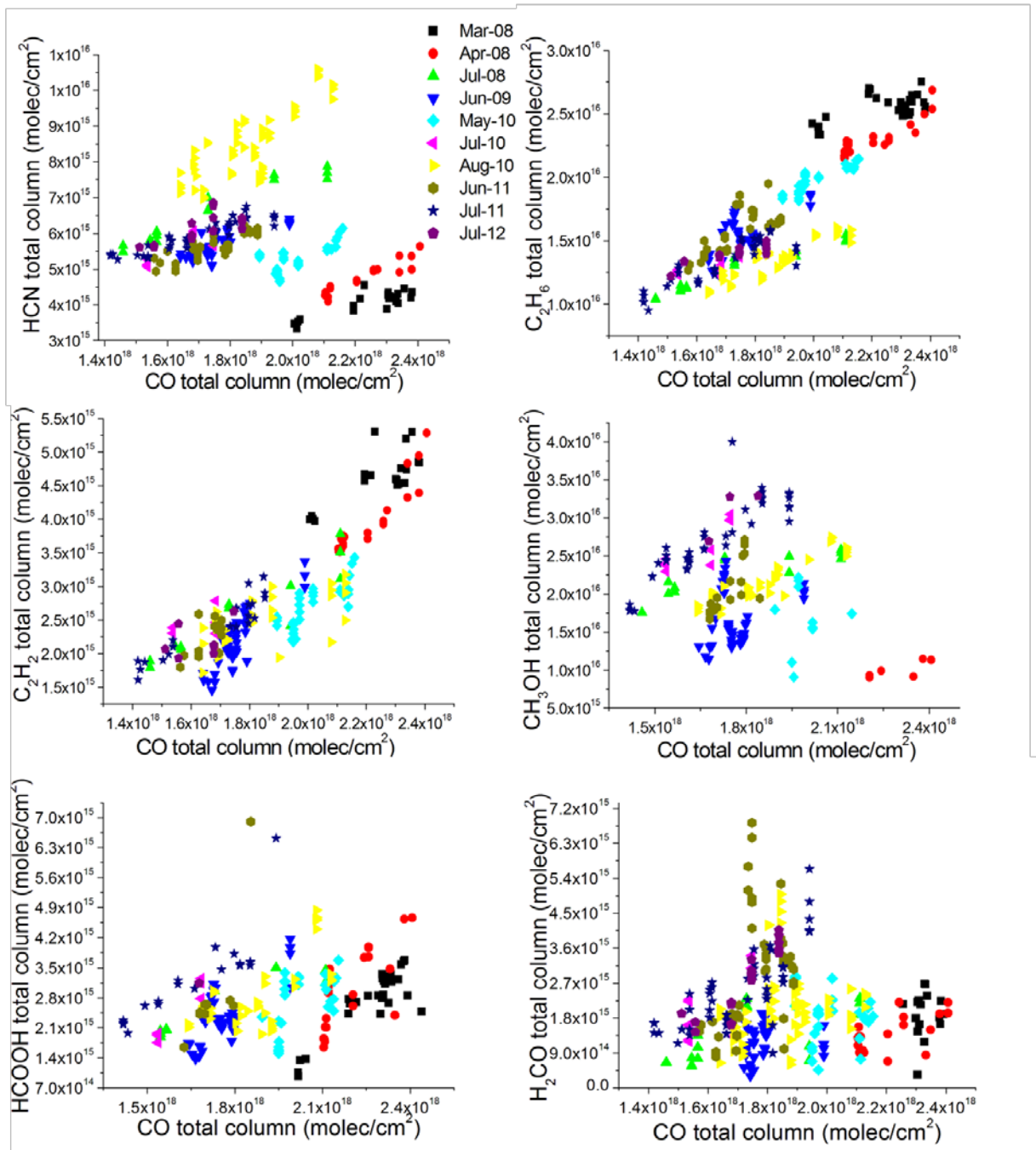


1043

1044 Figure 6: Timeseries of CO, HCN, C<sub>2</sub>H<sub>6</sub>, C<sub>2</sub>H<sub>2</sub>, CH<sub>3</sub>OH, and H<sub>2</sub>CO total columns measured by the  
 1045 FTIRs at Eureka (blue) and Thule (green) and calculated by MOZART-4 at Eureka (black) and  
 1046 Thule (red) for the August 2010 fire event.

1047

1048

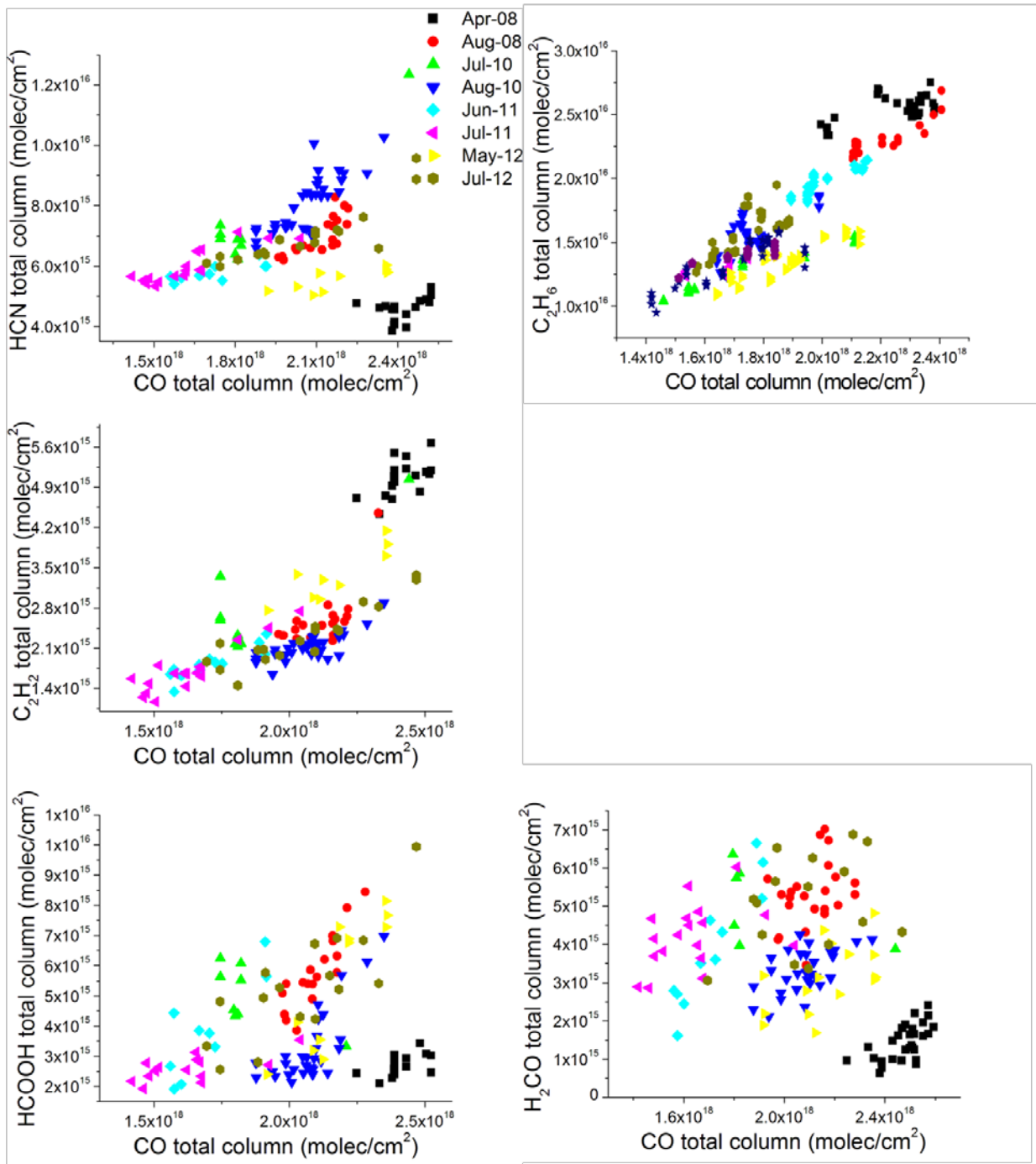


1049

1050 Figure 7: Scatter plots of the total columns of the target species (HCN, C<sub>2</sub>H<sub>6</sub>, C<sub>2</sub>H<sub>2</sub>, CH<sub>3</sub>OH,  
 1051 HCOOH, and H<sub>2</sub>CO) relative to CO for the ten fire events detected at Eureka (2008-2012).

1052

1053

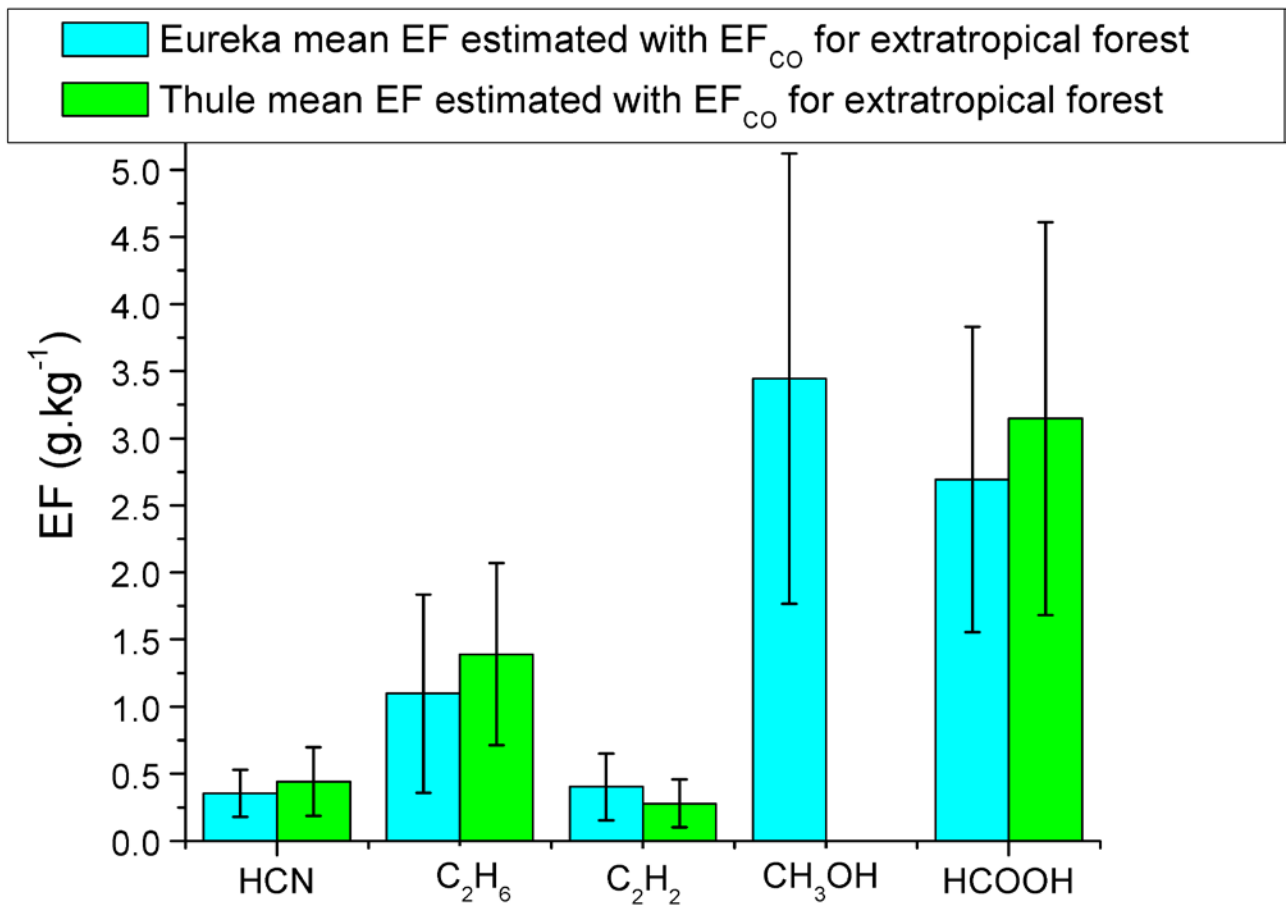


1054

1055 Figure 8: Scatter plots of the total columns of the target species (HCN, C<sub>2</sub>H<sub>6</sub>, C<sub>2</sub>H<sub>2</sub>, HCOOH, and  
 1056 H<sub>2</sub>CO) relative to CO for the eight fire events detected at Thule (2008-2012).

1057

1058

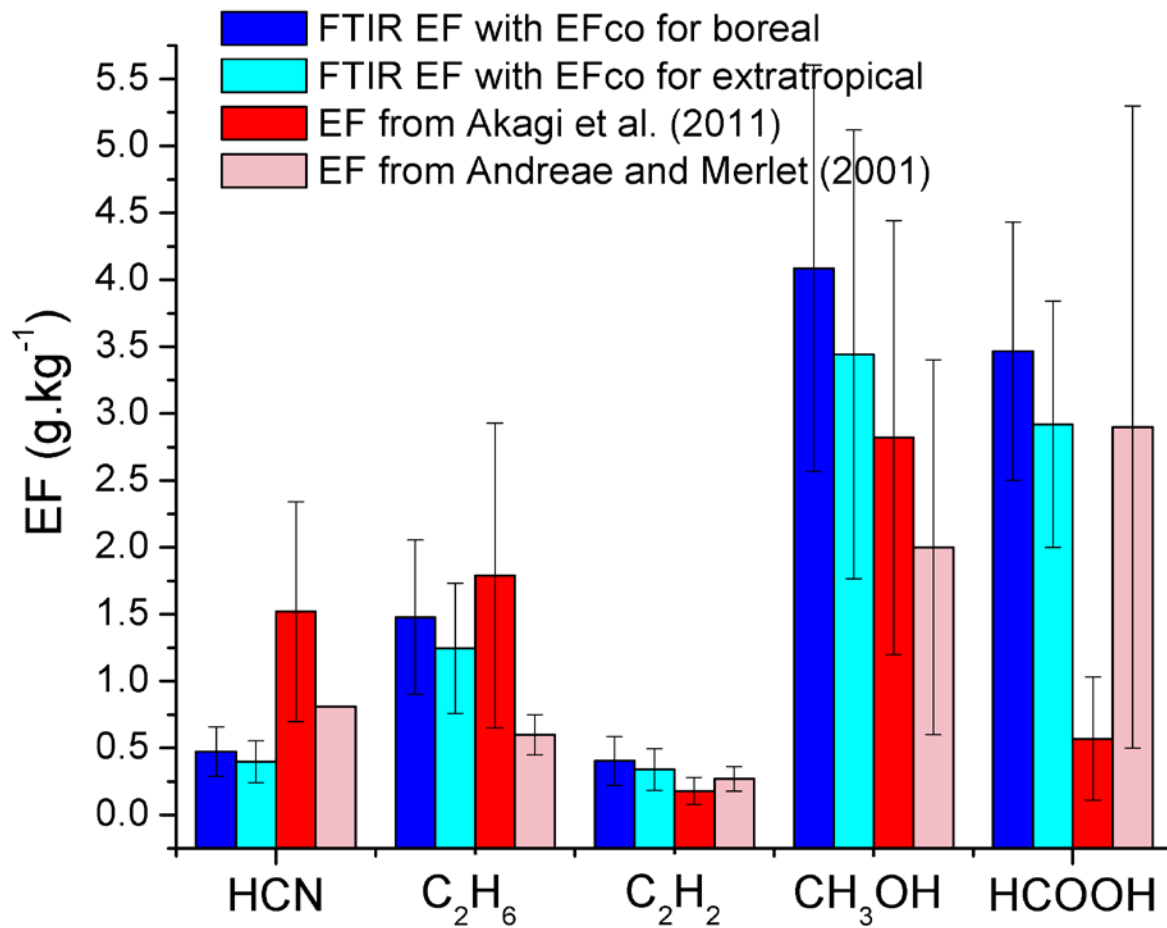


1059

1060 Figure 9: Emission factors calculated from the FTIR measurements performed at Eureka (cyan)  
 1061 and Thule (green), using EF<sub>CO</sub> of Andreae and Merlet (2001) for extratropical forest. Error bars  
 1062 correspond to the uncertainty in the CO emission factor and the uncertainty in the calculated  
 1063 regression slope, as well as the total uncertainties of the retrievals, all combined in quadrature.

1064

1065



1066

1067 Figure 10: Emission factors for boreal and extratropical EF<sub>CO</sub> calculated from FTIR measurements  
 1068 (blue and cyan), along with the emission factors found in the compilation studies of Akagi et al.  
 1069 (2011) (red) and Andreae and Merlet (2001) (pink).